ote technical note technic

Numerical Modeling of a Small Fire in an Aircraft Cargo Compartment Using the Fire Dynamics Simulator

October 2013

DOT/FAA/TC-TN13/17

This document is available to the U.S. public through the National Technical Information Services (NTIS), Springfield, Virginia 22161.

This document is also available from the Federal Aviation Administration William J. Hughes Technical Center at actlibrary.tc.faa.gov.

U.S. Department of Transportation

Federal Aviation Administration

NOTICE

This document is disseminated under the sponsorship of the U.S. Department of Transportation in the interest of information exchange. The U.S. Government assumes no liability for the contents or use thereof. The U.S. Government does not endorse products or manufacturers. Trade or manufacturers' names appear herein solely because they are considered essential to the objective of this report. The findings and conclusions in this report are those of the author(s) and do not necessarily represent the views of the funding agency. This document does not constitute FAA policy. Consult the FAA sponsoring organization listed on the Technical Documentation page as to its use.

This report is available at the Federal Aviation Administration William J. Hughes Technical Center's Full-Text Technical Reports page: actlibrary.tc.faa.gov in Adobe Acrobat portable document format (PDF).

Technical Report Documentation Page

1. Report No.	2. Government Accession No.	3. Recipient's Catalog No.
DOT/FAA/TC-TN13/17		

4. Title and Subtitle	5. Report Date
NUMERICAL MODELING OF A SMALL FIRE IN AN AIRCRAFT CARGO COMPARTMENT USING THE FIRE DYNAMICS SIMULATOR	October 2013
	6. Performing Organization Code
7. Author(s)	8. Performing Organization Report No.
Ezgi S. Oztekin	
9. Performing Organization Name and Address	10. Work Unit No. (TRAIS)
Technology and Management International, LLC (TAMI) 1433 Hooper Ave, Suite 330 Toms River, NJ 08405	
	11. Contract or Grant No.
12. Sponsoring Agency Name and Address	13. Type of Report and Period Covered
U.S. Department of Transportation Federal Aviation Administration Air Traffic Organization NextGen & Operations Planning Office of Research and Technology Development Washington, DC 20591	Technical Note
	14. Sponsoring Agency Code ANM-115

15. Supplementary Notes

The Federal Aviation Administration William J. Hughes Technical Center Aviation Research Division COR was Richard E. Lyon.

16. Abstract

According to Federal Aviation Regulations, fire and smoke detector devices installed in aircraft cargo compartments are required to alarm within the first 60 seconds of fire initiation. Expensive and time-consuming in-flight and ground tests are conducted to verify compliance and to grant approval for these detection systems. Although successful at fire detection, the detection systems are prone to detect airborne particles not associated with the fire; hence, they have high false alarm rates. Moreover, the same certification procedure is followed, regardless of the type of cargo compartment in which the detection systems are installed. In an attempt to minimize the number of certification tests required, to provide better guidelines for the certification process, and to improve the detector algorithms, the Federal Aviation Administration is evaluating computational fluid dynamics (CFD) as a tool to predict fire-induced flow behavior in aircraft cargo compartments.

The main objective of the current project was to assess the predictive abilities of available open-source CFD solvers for the transport of smoke and hot gases due to a small fire source in an enclosure. This report documents numerical simulations carried out using the Fire Dynamics Simulator, developed by the National Institute of Standards and Technology. The simulation results were compared with an extensive set of data collected from the fire tests of two cargo compartments, namely the forward cargo compartment of a Boeing 707 (B707) and the below-floor cargo compartment of a McDonnell Douglas DC-10 (DC10). There were four test cases, three of which were conducted in the B707 and differed only in the location of the fire source, while the last test case was performed in the DC10. The selected metrics for the comparison were the predictions of temperature, light transmission, and concentrations of carbon monoxide and carbon dioxide in the first 3 minutes of the test.

17. Key Words	18. Distribution Statement
Smoke detection, Small fire, Cargo compartment, Computational fluid dynamics (CFD)	This document is available to the U.S. public through the National Technical Information Service (NTIS), Springfield, Virginia 22161. This document is also available from the Federal Aviation Administration William J. Hughes Technical Center at actlibrary.tc.faa.gov.

19. Security Classif. (of this report)	20. Security Classif. (of this page)	21. No. of Pages	22. Price
Unclassified	Unclassified	44	

Form DOT F 1700.7 (8-72) Reproduction of completed page authorized

TABLE OF CONTENTS

	Page
EXECUTIVE SUMMARY	x
INTRODUCTION	1
METHODOLOGY	2
EXPERIMENTAL SECTION	2
Test Configurations	2
The Boeing 707	2
The McDonnell Douglas DC10	3
Fire Source	4
Experimental Uncertainty	6
NUMERICAL SECTION	6
Governing Equations	6
MODEL SETUP	7
Geometry and Grid	7
The B707	7
The DC10	9
Initial and Boundary Conditions	10
Wall Material Properties	10
Radiative Fraction	10
Validation Metrics	10
RESULTS	11
Comparisons With the Test Data	11
Test Case 1—B707 Base Fire	11
Test Cases 2 and 3—B707 Corner and Side Fires	16
Test Case 4—DC10 Base Fire	24

Summary of Model Results 27

CONCLUSIONS 30

REFERENCES 32

LIST OF FIGURES

Figure		Page
1	Forward Cargo Compartment of the B707	3
2	Below-Floor Cargo Compartment of the DC10	5
3	Fire Source: Resin Block Used as a Fire Source in the Full-Scale Tests and CO-to-CO_2 Ratio Measured in the Cone Calorimeter and During the Full-Scale Tests of the B707 Cargo Compartment	6
4	Model Geometry for the B707 Compartment	8
5	Computational Mesh for Baseline Fire Scenario for the B707 Compartment	8
6	Model Geometry for the DC10 Compartment	9
7	Computational Mesh for Baseline Fire Scenario for the DC10 Compartment	9
8	The B707 Base Fire: Comparisons Between Experimental Data and Model (FDS) Predictions—Time Variation of Time-Averaged Ceiling Gas Temperatures; Experimental Data and Model Predictions	12
9	The B707 Base Fire: Comparisons Between Experimental Data and Model (FDS) Predictions—Spatial Variation of Time-Averaged Ceiling Gas Temperatures at 60 s and 90 s	13
10	The B707 Base Fire: Comparisons Between Experimental Data and Model (FDS) Predictions—Contourplots of Time-Averaged Ceiling Gas Temperatures at Selected Times for Experimental Data at 60 s and 90 s, and Model Predictions at 60 s and 90 s	13
11	The B707 Base Fire: Comparisons Between Experimental Data and Model (FDS) Predictions—Time Variation of CO and CO_2 Concentrations at Analyzer Locations Aft, Mid, and TC36	14
12	The B707 Base Fire: Comparisons Between Experimental Data and Model (FDS) Predictions—Time Variation of Light Transmissions at Ceiling Beam Detectors (Aft, Mid, and TC36) and Vertical Beam Detectors (High, Mid, Low)	15
13	The B707 Corner Fire: Comparisons Between Experimental Data and Model (FDS) Predictions—Time Variation of Time-Averaged Ceiling Gas Temperatures for Experimental Data and Model Predictions	17
14	The B707 Side Fire: Comparisons Between Experimental Data and Model (FDS) Predictions—Time Variation of Time-Averaged Ceiling Gas Temperatures for Experimental Data and Model Predictions	18

15 The B707 Corner Fire: Comparisons Between Experimental Data and Model (FDS) Predictions—Spatial Variation of Time-Averaged Ceiling Gas Temperatures at 60 s and 90 s 19

16 The B707 Corner Fire: Comparisons Between Experimental Data and Model (FDS) Predictions—Contourplots of Time-Averaged Ceiling Gas Temperatures at Selected Times for Experimental Data at 60 s and 90 s, and Model Predictions at 60 s and 90 s 19

17 The B707 Side Fire: Comparisons Between Experimental Data and Model (FDS) Predictions—Spatial Variation of Time-Averaged Ceiling Gas Temperatures at 60 s and 90 s 20

18 The B707 Side Fire: Comparisons Between Experimental Data and Model (FDS) Predictions—Contourplots of Time-Averaged Ceiling Gas Temperatures at Selected Times for Experimental Data at 60 s and 90 s, and Model Predictions at 60 s and 90 s 20

19 The B707 Corner Fire: Comparisons Between Experimental Data and Model (FDS) Predictions—Time Variation of CO and CO_2 Concentrations at AFT Analyzer Location; Side Fire: Comparisons Between Experimental Data and Model (FDS) Predictions—Time Variation of CO and CO_2 Concentrations at AFT Analyzer Location 21

20 The B707 Corner Fire: Comparisons Between Experimental Data and Model (FDS) Predictions—Time Variation of Light Transmissions at Ceiling Beam Detectors and Vertical Beam Detectors 22

21 The B707 Side Fire: Comparisons Between Experimental Data and Model (FDS) Predictions—Time Variation of Light Transmissions at Ceiling Beam Detectors and Vertical Beam Detectors 23

22 The DC10 Base Fire: Comparisons Between Experimental Data and Model (FDS) Predictions—Spatial Variation of Time-Averaged Ceiling Gas Temperatures at 60 s and 90 s 24

23 The DC10 Base Fire: Comparisons Between Experimental Data and Model (FDS) Predictions—Contourplots of Time-Averaged Ceiling Gas Temperatures at Selected Times for Experimental Data at 60 s and 90 s, and Model Predictions at 60 s and 90 s 25

24 The DC10 Base Fire: Comparisons Between Experimental Data and Model (FDS) Predictions—Time Variation of CO and CO_2 Concentrations at FWD, AFT, TC5 Analyzer Locations 26

25 DC10 Base Fire: Comparisons Between Experimental Data and Model (FDS) Predictions—Time Variation of Light Transmissions at Ceiling Beam Detectors and Vertical Beam Detector 5' 27

26 Comparisons Between Experimental Data and Model (FDS) Predictions—Nondimensional Peak Values for Ceiling Gas Temperatures, Smoke and Gas Concentrations, Vertical Gas Temperatures, and Heat Fluxes 29

LIST OF TABLES

Table		Page
1	Wall Material Properties	10
2	Measured Radiative Fractions for Selected Fuels	10
3	Summary of Agreement Between Model Predictions and Measurements	28

LIST OF ABBREVIATIONS AND ACRONYMS

B707	Boeing 707
CFD	Computational fluid dynamics
CO	Carbon monoxide
CO_2	Carbon dioxide
DC10	McDonnell Douglas DC-10
FAA	Federal Aviation Administration
FDS	Fire Dynamics Simulator
FTIR	Fourier Transform Infrared Spectroscopy
HRR	Heat release rate

EXECUTIVE SUMMARY

According to Federal Aviation Regulations, fire and smoke detector devices installed in aircraft cargo compartments are required to alarm within the first 60 seconds of fire initiation. Expensive and time-consuming in-flight and ground tests are conducted to verify compliance and to grant approval for these detection systems. Although successful at fire detection, the detection systems often detect airborne particles not associated with the fire; thus, they have high false alarm rates. Moreover, the same certification procedure is followed, regardless of the type of cargo compartment in which the detection systems are installed. In an attempt to minimize the number of certification tests required, to provide better guidelines for the certification process, and to improve the detector algorithms, the Federal Aviation Administration is evaluating computational fluid dynamics (CFD) as a tool to predict fire-induced flow behavior in aircraft cargo compartments.

The main objective of the current project was to assess the predictive abilities of available open-source CFD solvers for the transport of smoke and hot gases due to a small fire source in an enclosure. This report documents numerical simulations carried out using the Fire Dynamics Simulator (FDS), developed by the National Institute of Standards and Technology. The simulation results were compared with an extensive set of data collected from the fire tests of two cargo compartments; namely, the forward cargo compartment of a Boeing 707 (B707), and the below-floor cargo compartment of a McDonnell Douglas DC-10 (DC10). There were four test cases, three of which were conducted in a B707 and differed only in the location of the fire source, while the last test case was performed in a DC10. The selected metrics for the comparison were the predictions of temperature, light transmission, and concentrations of carbon monoxide and carbon dioxide in the first 3 minutes of the test.

For the test cases studied, CFD proved to be a powerful tool, producing good agreement with the majority of the available test data. For the concentration fields, FDS model predictions are not only within the range of experimental uncertainty, but also, in general, follow the experimental mean very closely. For the temperature field in degrees Kelvin (K), there is a consistent 2 to 3K difference between the model estimates and the test data for ceiling thermocouples, and up to a 5K difference for the thermocouples placed on the thermocouple tree. Although these differences are within the range of reported experimental uncertainty, improvements in the model—particularly in the implementation of the radiation source term and in the near-wall treatments—may be necessary. However, it is not certain that the aforementioned differences are entirely due to model limitations/experimental uncertainties, as there are also uncertainties in the model input. It is suggested that new experimental studies be conducted where the uncertainties in the model input, such as the radiative fraction of fuel source and the wall heat losses, are minimized.

INTRODUCTION

Federal Aviation Regulations mandate the use of certified smoke and fire detection devices in aircraft cargo compartments [1]. The certification process of these devices requires both in-flight and ground tests, which are expensive and time consuming. Furthermore, the detection systems, although successful at fire detection, are prone to detect airborne particles not associated with the fire; hence, they have high false alarm rates [2]. It is reported that only one in every hundred alarms is due to a real fire source [3 and 4]. False alarms lead to unnecessary evacuations, flight delays, and diversions from intended flight paths, and bring additional safety and cost concerns. Moreover, the same certification procedure is followed on any type of compartment regardless of its size or ventilation system. This practice is questionable because the smoke behavior will be different in a wide- or narrow-body compartment or in a compartment with or without ventilation. It is critical to have a better understanding of fire-induced flow behavior in enclosures to improve the reliability of the detection systems, to provide better guidelines for the certification process, and to reduce the number of necessary tests for certification. Although there is ongoing experimental research for this purpose, it is also important to use the available numerical modeling methods because of the scenario-specific nature and complexity of the problem.

The focus of the current study is to assess the predictive abilities of available computational fluid dynamics (CFD) tools when applied to buoyancy-driven flows due to temperature gradients in enclosures. The Fire Dynamics Simulator (FDS) [5], developed by the National Institute of Standards and Technology, was chosen over many open-source solver candidates, particularly for its fast turnaround time and robustness. The FDS solves governing equations of fluid motion for low Mach number thermally driven flow, specifically targeting smoke and heat transport from fires. It has been verified and validated for a number of fire scenarios [5].

Numerical simulations were conducted for a small fire with a maximum heat release rate (HRR) of 5 kW in the forward cargo compartment of a Boeing 707 (B707) and in the below-floor cargo compartment of a McDonnell Douglas DC-10 (DC10). For the B707 compartment, three fire scenarios were tested. All three fire scenarios, differing only in the location of the fire source, were modeled. The simulation results were compared with the existing full-scale tests with 44 thermocouples, 6 beam detectors and 3 gas analyzers. For the DC10 compartment, only one fire scenario was tested with 45 thermocouples, 4 beam detectors, and 3 gas analyzers. The selected metrics for the comparison were the predictions of temperature, light transmission, and concentrations of carbon monoxide (CO) and carbon dioxide (CO_2), in the first 3 minutes of the test.

METHODOLOGY

EXPERIMENTAL SECTION.

TEST CONFIGURATIONS.

In a collaborative effort between Sandia National Laboratories and the Federal Aviation Administration (FAA) William J. Hughes Technical Center, a CFD tool was developed over a 5-year period between 2003 and 2008, with the ultimate goal of improving and streamlining the certification process for aircraft cargo compartment smoke detection systems. As part of this project, a series of full- and bench-scale tests were conducted. The full-scale tests were performed on two types of compartments: the forward cargo compartment of a B707 and the below-floor cargo compartment of a DC10 [6, 7, and 8]. In addition, to characterize the fire source of the full-scale tests, bench-scale tests and cone calorimetry with Fourier Transform Infrared Spectroscopy (FTIR) were also conducted [9 and 10]. We use the same set of test data both in the analysis and in the preparation of our model setup. The information presented in this section is a brief summary of the experiments and is provided only for completeness. Neither the full-scale nor the bench-scale tests were repeated within the framework of the current study. Further details of both the full-scale and bench-scale tests can be found in numerous previous reports and in references 6 through 10 of this report.

The Boeing 707. The B707 is a narrow-body aircraft. Its forward cargo compartment does not have forced ventilation. In addition, the natural ventilation due to the pressure differential close to the door area was negligibly small (~0.008 m^3/s). Its walls, including the floor and the ceiling, are insulated with cargo liner (i.e., fiberglass epoxy resin). The front view and top view of the compartment are shown in figure 1(a and b), respectively. The total volume of the compartment is approximately 25.8 m^3, with dimensions of 3.2 x 1.4 x 6.7 m^3 in length *x* width *x* depth.

For the B707, three fire scenarios were tested: baseline, corner, and side fires. For each scenario (which differed only as far as the fire location), temperature, smoke obscuration, and gas-species concentrations were measured. The locations of each device relative to the fire source are shown in the schematic of the top view of the compartment (figure 1(b)). Most of the diagnostic devices were placed close to the ceiling, except for the three smokemeters and four thermocouples that were positioned vertically. There were 40 ceiling thermocouples laid out on a 5 x 8 grid, shown with circles and numbered from 1 to 40 (TC_1 to TC_{40}) in the figure. There were three ceiling smokemeters, labeled as forward (SMK FWD), mid (SMK MID), and aft (SMK AFT) smokemeters, and three smokemeters 1 foot apart from one another in the vertical (*z*) direction (SMK VERT). Two of the gas analyzers were located in the recessed areas on each side of the baseline fire source and the third was placed close to TC_{36}. The recessed areas, shown inside the dotted lines in figure 1(b), were 0.08 m high and ~0.3 m wide. The thermocouple tree was located at x = -0.08 m, y = 3.66 m, shown with an X in figure 1(b), and four thermocouples were positioned vertically 1 foot apart from one another. Moreover, heat flux gauges, in two colors (black and orange), were used at two locations—one directly above the baseline fire (x = 0.08 m, y = 3.73 m) and another was 1.5 m away from the fire (x = 0.08 m, y = 5.27 m). There was no forced ventilation for the B707 cargo compartment; however, a 0.1-m diameter

duct was used in the experiments to simulate leakage through doors due to the pressure differential.

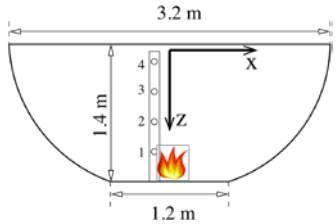

(a) Front View

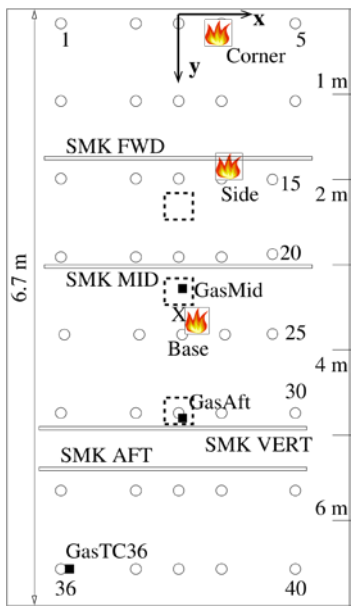

(b) Top View

Figure 1. Forward Cargo Compartment of the B707

<u>The McDonnell Douglas DC10</u>. The DC10 is a wide-body aircraft. The below-floor cargo compartment, having approximately 99 m^3 volume, is four times larger than the B707 compartment studied. The dimensions of the compartment are 4.4 x 1.7 x 14.0 m^3 (length *x* width *x* depth). Unlike the B707 compartment, it has a considerable amount of forced ventilation through two air inlet ports located on the ceiling. The total amount of forced ventilation is ~0.19 m^3/s. In addition, the compartment door, which opens upward, is curved, creating an escape area for hot gases and allowing leakage, resulting in a natural ventilation of ~0.04 m^3/s. All the walls of the compartment, including the floor and the ceiling, are made up of weathered galvanized steel. The front view and top view of the compartment are shown in figure 2(a and b).

For the DC10, only one fire scenario (baseline fire) was tested. Similar to the B707 tests, temperature, smoke obscuration, and gas-species concentrations were measured. Although measurements for heat flux and temperatures existed in the vertical, their locations were not

recorded and were unclear. A schematic of the compartment and locations of each device relative to the fire source, viewed from the top, is shown in figure 2(b). There were 45 ceiling thermocouples laid out on a 5 x 9 grid, in addition to the four smokemeters and three gas analyzers. The four ceiling smokemeters are labeled as forward (SMK FWD), mid (SMK MID), aft (SMK AFT) and 5′ (SMK 5′), according to their location. Two of the gas analyzers were located in the recessed areas and the third one was placed close to TC_5. The recessed areas, shown as dotted squares in figure 2(b), were 0.05 m high and ~0.4 m wide. The ceiling air-inlet vents are located at 4.7 and 9.5 m; both have identical cross-sectional areas of 0.23 x 0.09 m^2, shown as filled rectangles in figure 2(b). The exhaustive list of instrument locations for both B707 and DC10 cargo compartment tests can be found in reference 7.

FIRE SOURCE.

The standardized fire source developed by the FAA Fire Safety Branch was used in all of the experiments. The fire source locations corresponding to the three fire scenarios studied for the B707 compartment and the baseline fire scenario for the DC10 compartment are shown in figures 1(b) and 2(b), respectively, as "Base," "Side," and "Corner." The FAA fire source is a compressed plastic resin block designed to yield combustion products similar to the actual luggage fires (figure 3(a)). It has an embedded nichrome wire to enable remote ignition [9 and 10]. The HRR, the mass loss rate, and the production rates of gas species and smoke were measured using cone calorimetry with FTIR. From these measurements, the time-dependent yields of CO, CO_2, and soot of the burning specimen were calculated. The mean values for CO, CO_2, and soot yields were approximately 0.065, 1.25, and 0.125, respectively. The model input used in the previous modeling efforts was based on the FTIR data [6 and 10]; however, CO yields measured from the FTIR and the cone calorimeter were different. For the results presented in this report, the direct measurements from cone calorimetry were adopted. The CO/CO_2 ratios measured in the cone calorimetry and in the full-scale tests are shown in figure 3(b). The average ratio is displayed in a solid line for the cone calorimetry and in symbols for the full-scale tests of the B707 cargo compartment. The CO/CO_2 ratios are comparable, indicating that ventilation characteristics of the bench-scale and the full-scale tests were similar. Thus, it is appropriate to use cone calorimetry test data to represent the burning behavior in the full-scale tests.

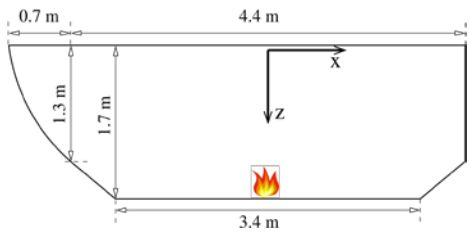

(a) Front View

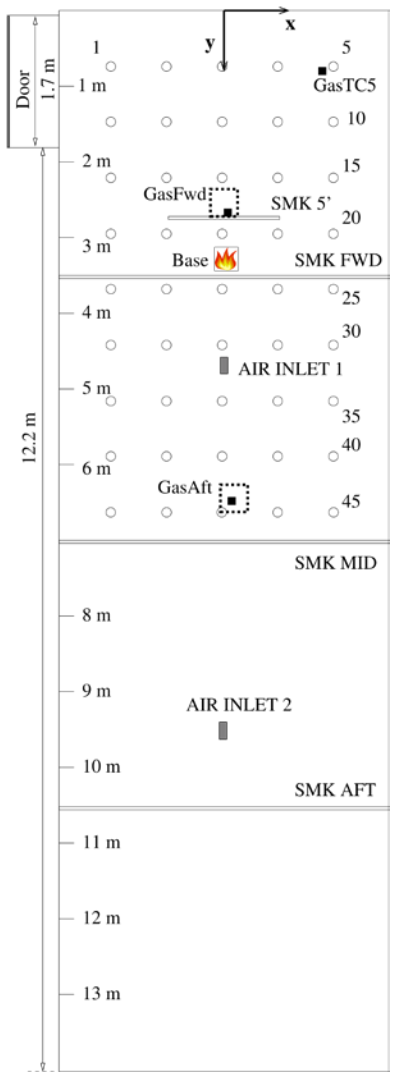

(b) Top View

Figure 2. Below-Floor Cargo Compartment of the DC10

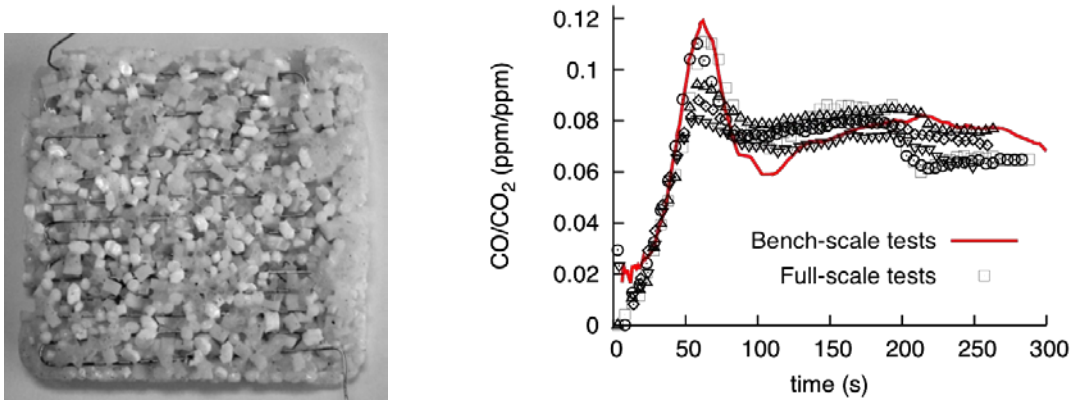

(a) Resin Block (b) CO-to-CO_2 Ratio

Figure 3. Fire Source: (a) Resin Block Used as a Fire Source in the Full-Scale Tests and (b) CO-to-CO_2 Ratio Measured in the Cone Calorimeter and During the Full-Scale Tests of the B707 Cargo Compartment

EXPERIMENTAL UNCERTAINTY.

Tests were repeated for each compartment and for each fire scenario to determine the experimental uncertainty. The baseline experiments were comprised of 15 full-scale tests for both B707 and DC10 compartments, while the side and corner fire scenarios of the B707 compartment each consisted of three tests. The CO and CO_2 analyzer locations were changed for every five baseline fire tests. The uncertainty in the measurements were reported to be 1K to 6K, depending on the proximity to the fire for ceiling temperatures in degrees Kelvin (K)—more than 10 and 100 ppm, respectively, for CO and CO_2 concentrations [7 and 8]. The uncertainty in the light transmissions was also reported to increase greatly for values below 80% [8]. In the comparisons with the model results in this report, the ensemble average of the tests are used. Note that, since the ambient temperature is not the same for all tests because of seasonal temperature differences, the rise in temperatures, instead of the absolute value, was used in the calculation of the ensemble averages.

NUMERICAL SECTION.

The numerical simulations are performed using the FDS [5 and 11]. The FDS is a second-order accurate finite difference-solver with explicit time integration. It is based on a low Mach number flow formulation with a mixture fraction combustion model and Smagorinsky turbulence model. It solves the radiation transport equation for gray nonscattering medium. It implements the Werner and Wengle wall model and also has options to model one-dimensional pyrolysis and heat conduction.

GOVERNING EQUATIONS.

The FDS is based on the following system of equations derived for ideal gas flows driven by a localized heat addition in the gravity field [5 and 11]:

$$\frac{\partial \rho}{\partial t} + \nabla \cdot (\rho u) = 0$$

$$\frac{\partial (\rho Y_\alpha)}{\partial t} + \nabla \cdot (\rho Y_\alpha u) = -\nabla \cdot J_\alpha + \omega_\alpha \tag{1}$$

$$\frac{\partial (\rho u)}{\partial t} + \nabla \cdot (\rho u u) = -\nabla \cdot p^* + \rho g$$

$$\frac{\partial (\rho h)}{\partial t} + \nabla \cdot (\rho h u) = Dp_o / Dt + Q - \nabla \cdot q$$

$$p_o = \rho R T$$

where Q is the heat source, ω_α is the αth species production rate, and $D/Dt = \frac{\partial}{\partial t} + u \cdot \nabla$ is the material derivative. The diffusive mass flux is defined as $J_\alpha = \rho D_\alpha \nabla Y_\alpha$, with the mass diffusivity D. The heat flux is $q = -k \cdot \nabla T - \sum_\alpha h_\alpha J_\alpha + q_r$, with the thermal conductivity, k, and the radiative heat flux, q_r. Note that energy conservation is written in terms of sensible enthalpy, $h = \sum_\alpha h_\alpha J_\alpha$, where $h_\alpha = \int c_{p_\alpha} dT$. Note also that the above equations are based on inviscid flow formulations [11]. The turbulence description is added by modeling the subgrid-scale dissipative processes, either by constant or dynamic coefficient Smagorinsky model [12] in the Large Eddy Simulation framework of the solver [5].

In FDS, pressure is decomposed into two components: thermal and dynamic pressures. The thermal pressure, p_o, is related with density and temperature through the equation of state, while the dynamic pressure, p^*, drives the fluid motion. This decomposition relaxes the time-step requirement by filtering out the acoustic waves. It also eliminates the need for direct solution of the energy equation. Instead, velocity divergence is formulated from thermodynamic quantities by combining the conservation of mass and energy with the equation of state, and the total dynamic pressure is computed using a direct solver for the Poisson equation [5 and 13].

Further details of the solver and its applications on a wide array of validation/verification cases can be found in FDS technical documentation [5].

MODEL SETUP.

GEOMETRY AND GRID.

The B707. The cargo compartment of a B707 is a closed, long, rectangular prism with curved sidewalls and three recessed areas on the ceiling, as shown in figure 4. It is 6.7 m long, 1.4 m high, and ~3.2 m wide. In figure 5(a and b), the rectilinear, single-domain computational mesh is shown in the *x-y* and *y-z* planes, respectively. The temperature contours are plotted only

to show the extent of the flow field in the vertical and the location of the baseline fire source. Note that the height of the computational domain increases to 1.5 m when recessed areas are included. The grid is stretched in the ~0.4 m area of the fire source in both lateral (x) and longitudinal (y) directions. For the side and corner fire configurations, the stretched mesh is shifted so as to resolve the heat source and the associated flow field gradients. The grid dimensions in the x, y, and z directions are 132 x 144 x 72, respectively. The minimum grid spacing is 0.022 m, while the maximum is ~0.2 m in the y-direction. The characteristic fire diameter, $D^* = \left(\frac{\dot{Q}}{\rho_\infty c_p T_\infty \sqrt{g}} \right)$, is ~ 0.11 m, where $\dot{Q}$ is the total HRR and ρ_∞, c_p, and T_∞ are the density, specific heat capacity, and temperature of the ambient flow, respectively. Accordingly, the ratio of characteristic fire diameter to minimum grid spacing is $D^*/\Delta x_{min} \approx 5$.

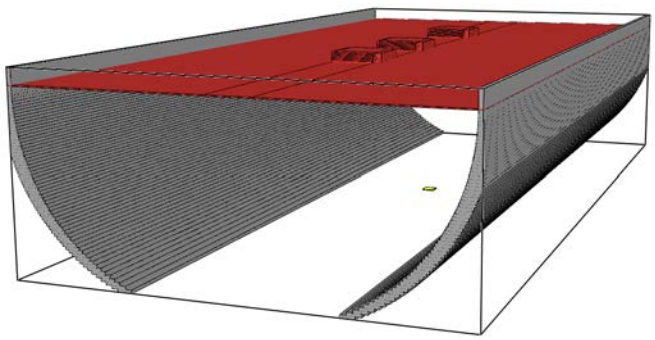

Figure 4. Model Geometry for the B707 Compartment

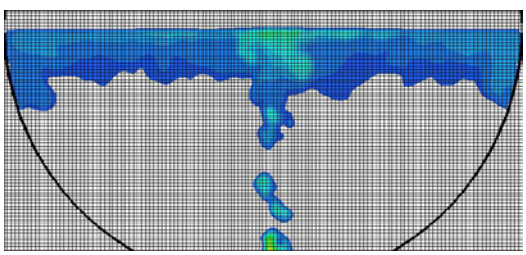

(a) *X-Z* Plane

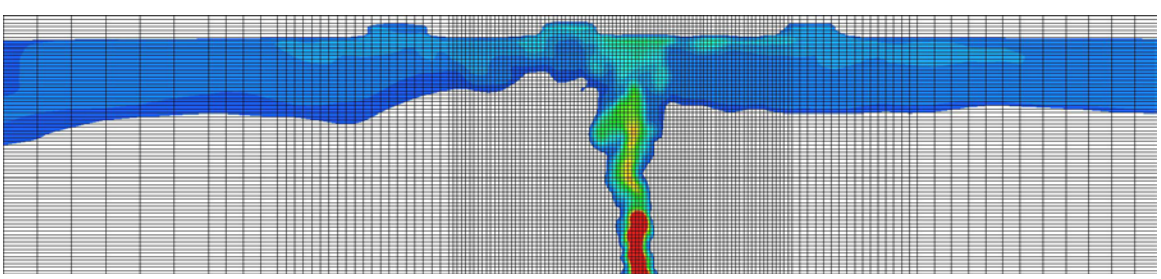

(b) *Y-Z* Plane

Figure 5. Computational Mesh for Baseline Fire Scenario for the B707 Compartment

The DC10. Unlike the B707 compartment, the DC10 has straight walls with a slope near the floor shaped to fit into a circular aircraft exterior. The compartment door is curved (shown in green in figure 6) and is 14.0 m long, 1.7 m high, and ~5.6 m wide. The rectilinear, single-domain computational mesh is depicted in the *x*-*y* and *y*-*z* planes of figure 7(a and b), respectively. The height of the computational domain increases to 1.8 m when recessed areas are included. The grid is stretched in the ~0.8 m area of the fire source in lateral (*x*) and longitudinal (*y*) directions. The grid dimensions in the *x*, *y*, and *z* directions are 135 x 240 x 81, respectively. The minimum grid spacing is 0.022 m, while the maximum is ~0.2 m in the *y*-direction. The ratio of characteristic fire diameter to minimum grid spacing is $D^*/\Delta x_{min} \approx 5$.

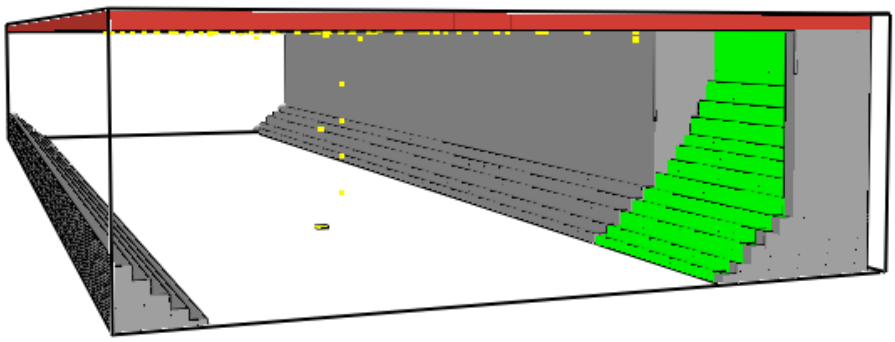

Figure 6. Model Geometry for the DC10 Compartment

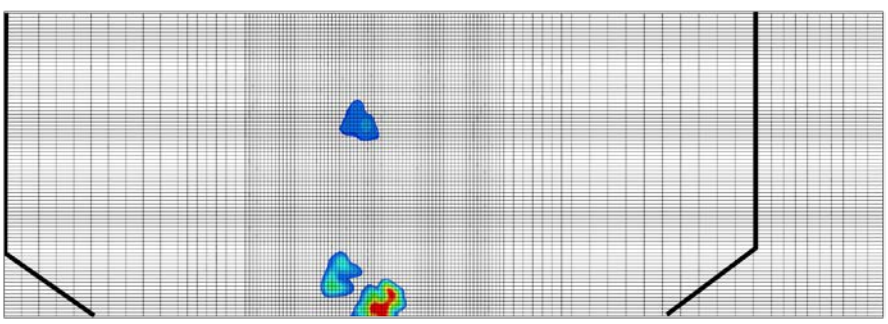

(a) *X*-*Z* Plane

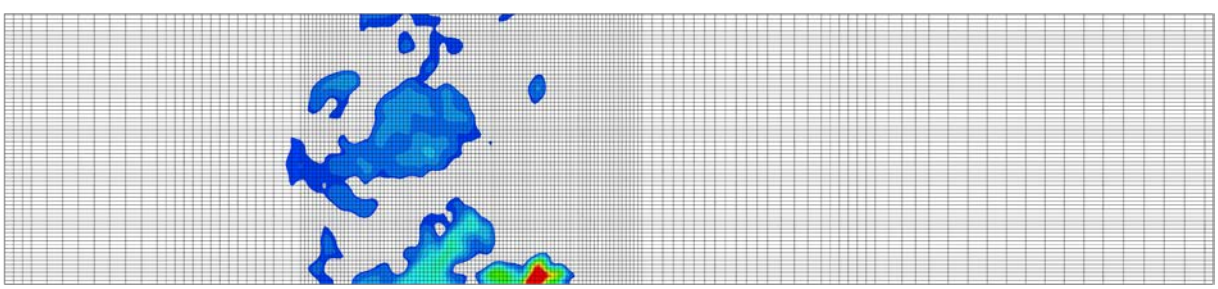

(b) *Y*-*Z* Plane

Figure 7. Computational Mesh for Baseline Fire Scenario for the DC10 Compartment

INITIAL AND BOUNDARY CONDITIONS.

Wall Material Properties. All walls are assumed to be cargo liner made up of fiberglass epoxy resin for the B707, and weathered, galvanized steel for the DC10. A specimen sample was sent for testing to obtain the thermal properties of the B707 cargo liner. The wall material properties of the DC10 are assumed to be similar to those of steel. The walls are assumed to have 0.85 emissivity for the DC10 compartment. Note that the ceiling wall is very thin in both cases (0.58 mm for the B707 and 1 mm for the DC10). The properties of the wall material used in the simulations for both compartment types are shown in table 1, where k is conductivity, ρ is density, c_p is specific heat capacity, and ε is emissivity.

Table 1. Wall Material Properties

Property	B707	DC10
ρ (kg/m^3)	1694	7850
k (W m^{-1} K^{-1})	0.25	45.8
c_p (J kg^{-1} K^{-1})	1000	460
ε	1.00	0.85

Radiative Fraction. Radiative fraction was determined based on the fact that it increases with the sooting propensity of the fuel. The soot yield (Y_S) of the fire source was measured to be 0.125 in the cone calorimeter [9 and 10]. A list of measured radiative fractions, χ_R, for fuels with similar soot yield values is shown in table 2 [14]. The table suggests a minimum radiative fraction of 0.55, consistent with the heat flux measurements.

Table 2. Measured Radiative Fractions for Selected Fuels [14]

Fuels	Y_S (g/g)	χ_R
Thiophenol	0.122	0.55
1-3 Butadiene	0.125	0.54
Aniline	0.120	0.55
Polyethylene with chlorine	0.115	0.56

VALIDATION METRICS.

The validation metrics were chosen as the temperatures, the CO and CO_2 concentrations, and the light transmissions at the corresponding instrument locations of the full-scale tests. Temperature comparisons were made using the modeled thermocouple readings as opposed to the true temperatures. The thermocouple temperatures are computed directly by solving the energy equation for a given thermocouple defined by the properties of its bead (i.e., diameter, density, emissivity, and specific heat) [15]. The default bead property set in FDS is used for the results obtained in this report. Because the experimental data for gas concentrations are provided in

volume fractions, comparisons for gas concentrations are also made in terms of volume fractions. FDS does not have a direct output for light transmissions but, per user request, it calculates obscurations. The light transmissions, defined below, are computed from the obscuration output data:

$$LT = \exp\left(-K_m \sum_{i=1}^{N} \rho_{soot,i} \Delta x_i / L \right) \cdot 100(\%) \tag{2}$$

where L^* is in feet and obscuration is (1- LT) 100 (%). The mass extinction coefficient, K_m, is to be 7600 m^2/kg, suggested for flaming combustion in the literature [16].

RESULTS.

COMPARISONS WITH THE TEST DATA.

For all four test cases studied, the same set of flow quantities (temperature and concentration fields) were examined. Comparisons between the model solution and the experimental data are presented in two groups: first, the time variation at selected locations; second, the spatial variations at selected times.

Test Case 1—B707 Base Fire. For test case 1 (the B707 base fire), figures 8 to 10 show comparisons of thermocouple readings, figure 11 displays comparisons of CO and CO_2 concentrations, and figure 12 shows comparisons of smoke concentrations. In general, model predictions for the ceiling gas temperatures agreed with the test data. Those above the fire were slightly underestimated, while those away from it were slightly overestimated (figures 8-10). On the other hand, solutions for vertical gas temperatures (not shown), which were overpredicted at all four locations, disagreed with the test data when measured a foot apart from each other on a thermocouple tree located close to the fire. The discrepancy close to the floor can be explained by the model treatment of the radiation source term and inadequate grid resolution in this region. However, the disagreement for the thermocouple readings close to the ceiling is suspected to be due to faulty instrumentation, and requires further experimental analysis. The treatment of the radiation source term also affected the ceiling wall temperature directly above the fire. The wall temperature at this location was underpredicted (not shown) and resulted in a lower heat flux estimate in comparison to the measured value (not shown). Solutions for wall temperatures, and thereby for heat fluxes, are more reliable away from the fire source. The concentrations of CO, CO_2, and smoke were reasonably well predicted and followed the experimental mean very closely (figures 11 and 12).

---

* For the B707: 10.42 feet for ceiling and 9.83, 9.08, and 6.82 feet for vertical high, mid, and low beam detectors, respectively. For the DC10: 10.42 feet for ceiling and 9.83, 9.08, and 6.82 feet for vertical high, mid, and low beam detectors, respectively.

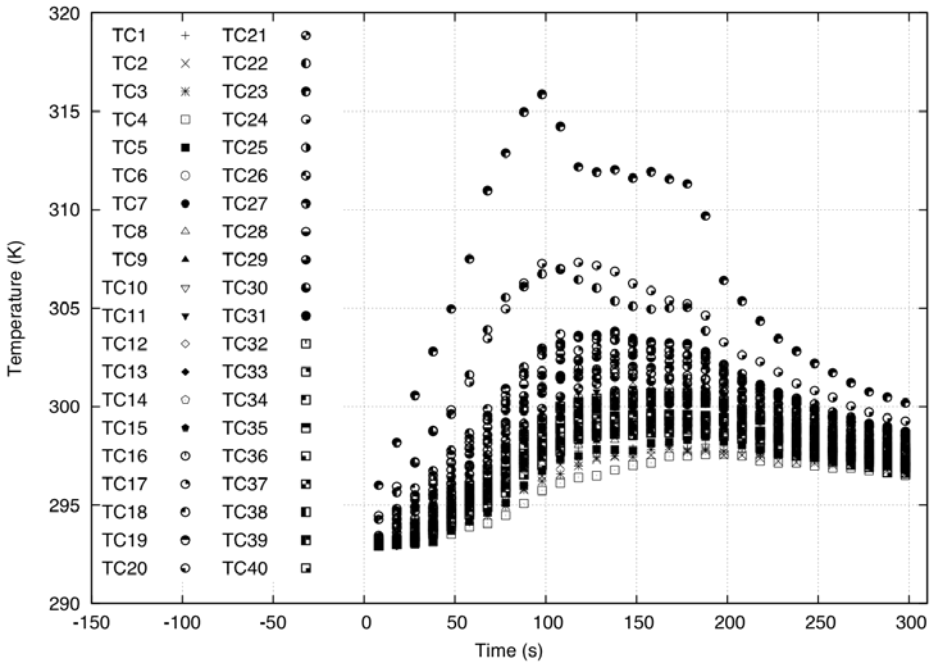

(a) Experimental Data

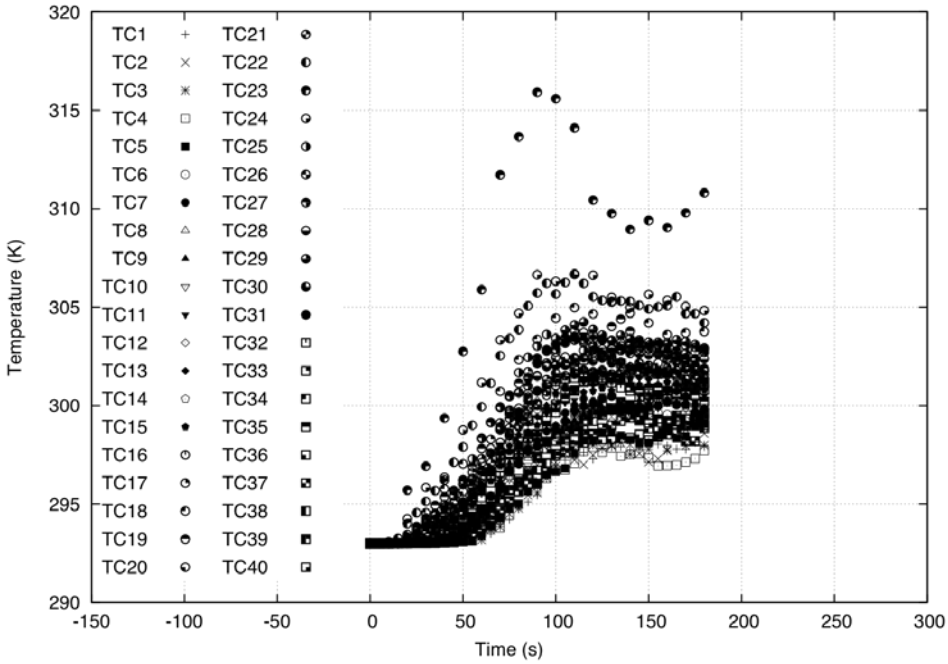

(b) Model (FDS) Predictions

Figure 8. The B707 Base Fire: Comparisons Between Experimental Data and Model (FDS) Predictions—Time Variation of Time-Averaged Ceiling Gas Temperatures; (a) Experimental Data and (b) Model Predictions

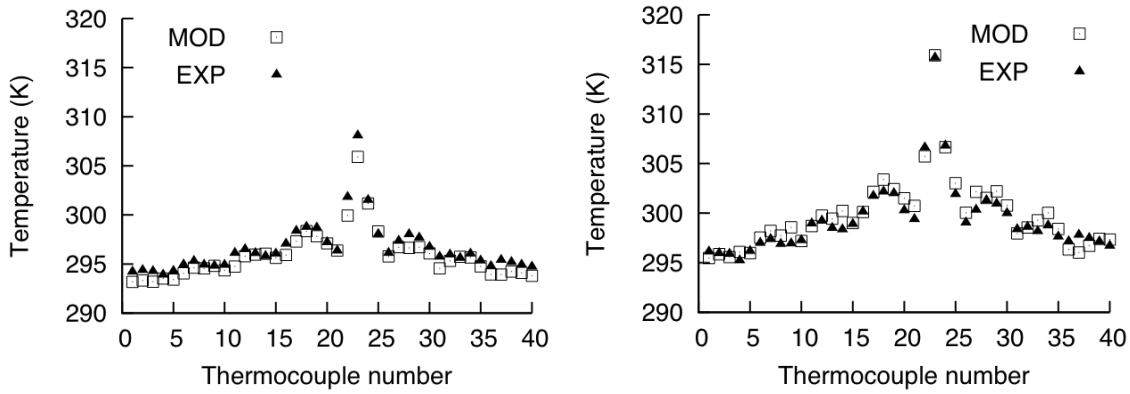

(a) 60 s (b) 90 s

Figure 9. The B707 Base Fire: Comparisons Between Experimental Data and Model (FDS) Predictions—Spatial Variation of Time-Averaged Ceiling Gas Temperatures at (a) 60 s and (b) 90 s

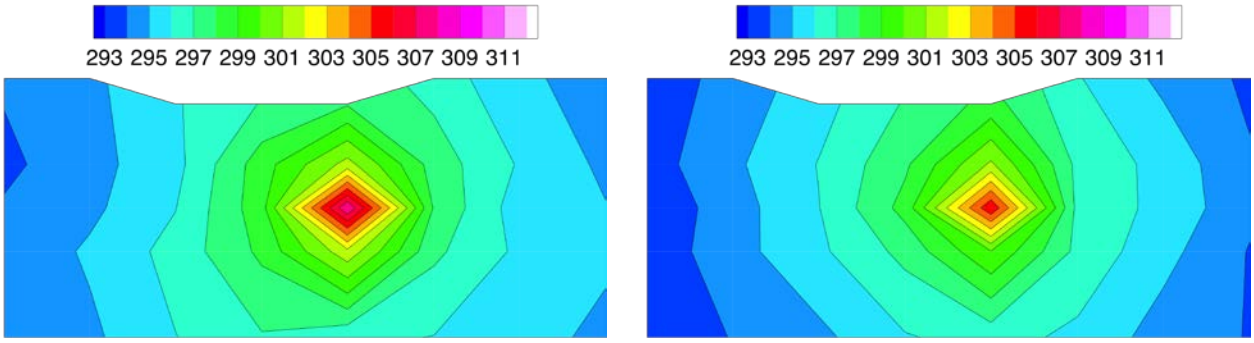

(a) 60 s (EXP) (b) 60 s (MOD)

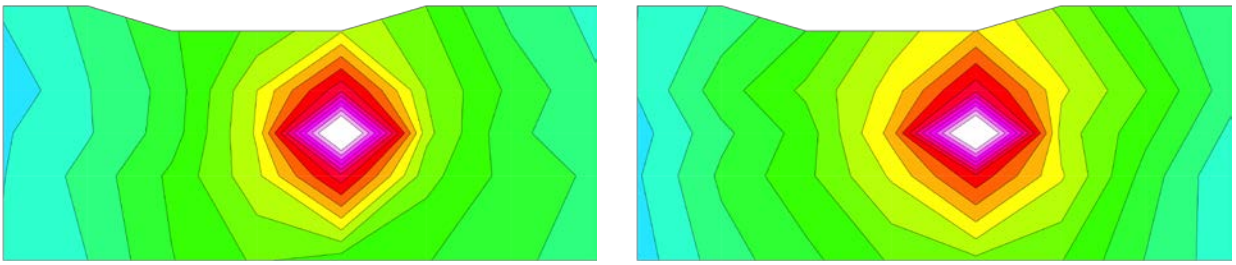

(c) 90 s (EXP) (d) 90 s (MOD)

Figure 10. The B707 Base Fire: Comparisons Between Experimental Data and Model (FDS) Predictions—Contourplots of Time-Averaged Ceiling Gas Temperatures at Selected Times for Experimental Data at (a) 60 s and (c) 90 s, and Model Predictions at (b) 60 s and (d) 90 s

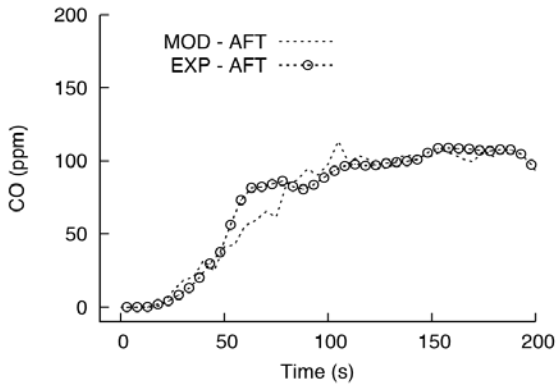

(a) CO - AFT

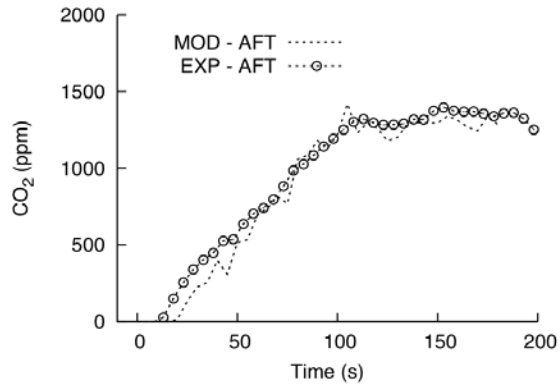

(b) CO_2 - AFT

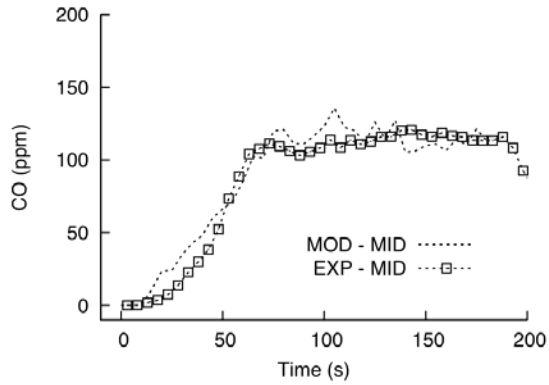

(c) CO - MID

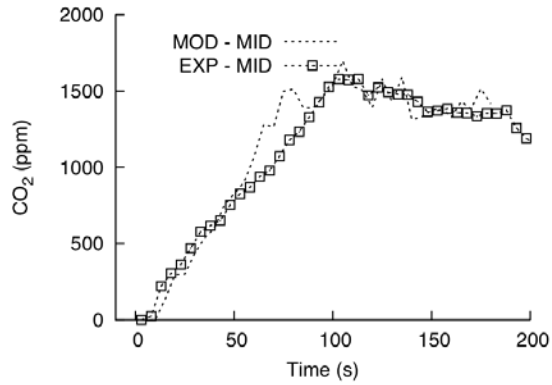

(d) CO_2 - MID

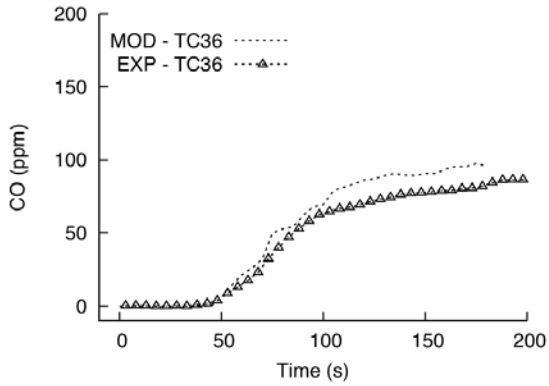

(e) CO - TC36

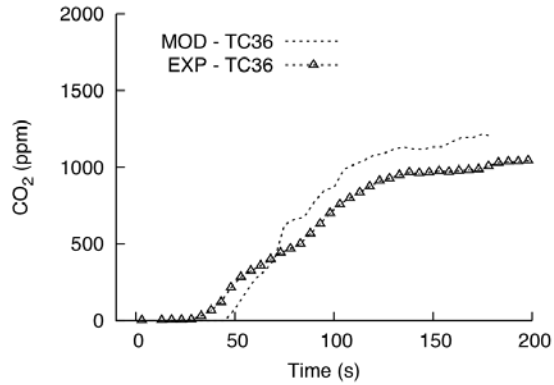

(f) CO_2 - TC36

Figure 11. The B707 Base Fire: Comparisons Between Experimental Data and Model (FDS) Predictions—Time Variation of CO and CO_2 Concentrations at Analyzer Locations (a and b) Aft, (c and d) Mid, and (e and f) TC36, Respectively

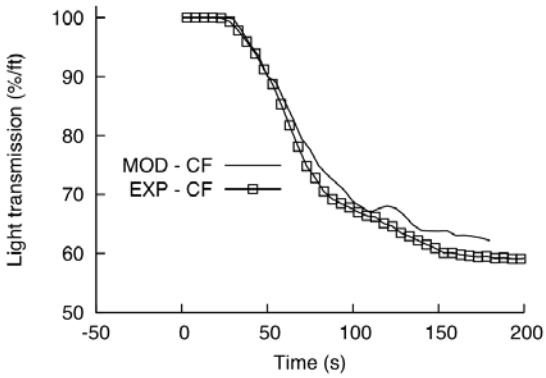

(a) Ceiling - FWD

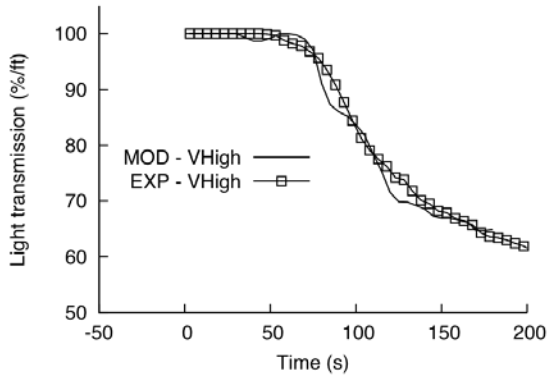

(b) Vertical - HIGH

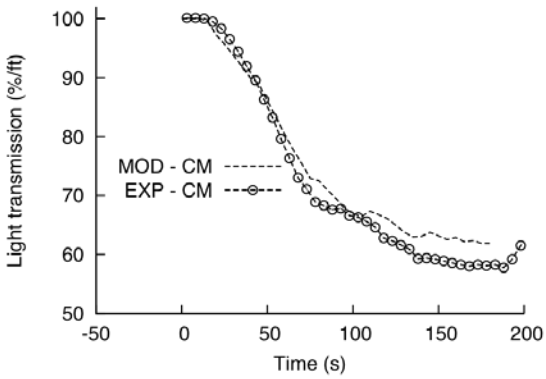

(c) Ceiling - MID

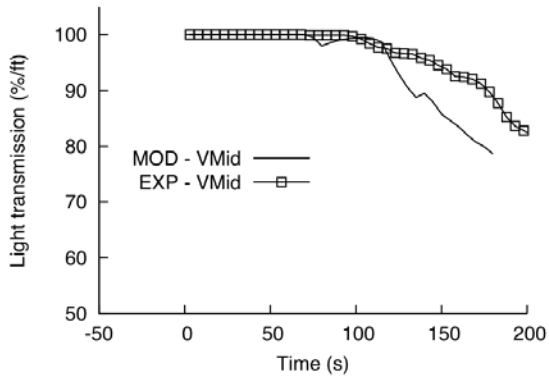

(d) Vertical - MID

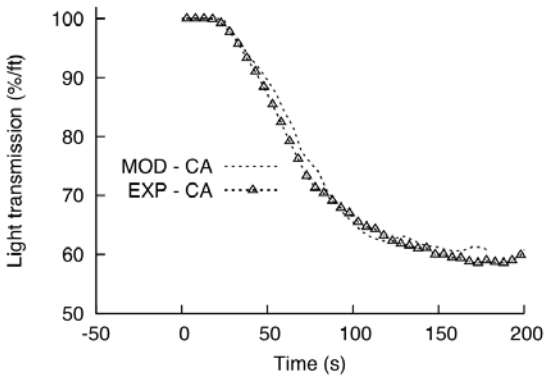

(e) Ceiling - TC36

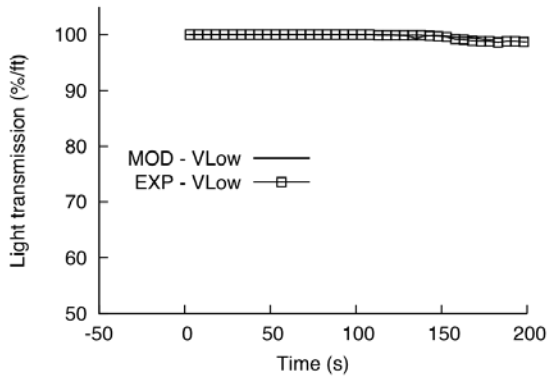

(f) Vertical – LOW

(CF: ceiling forward, CM: ceiling mid, CA: ceiling aft, VHigh: vertical high, VMid: vertical mid, VLow: vertical low)

Figure 12. The B707 Base Fire: Comparisons Between Experimental Data and Model (FDS) Predictions: Time Variation of Light Transmissions at Ceiling Beam Detectors: (a) Aft, (c) Mid, and (e) TC36; and Vertical Beam Detectors: (b) High, (d) Mid, (f) Low

Test Cases 2 and 3—B707 Corner and Side Fires. For the other two test cases of the B707 cargo compartment, model predictions portray a very similar picture to that for test case 1, except for the increase in the predicted temperature values. Figures 13, 15, and 16 and figures 14, 17, and 18 compare the temperature predictions with the measured data for test case 2 (B707 corner fire) and test case 3 (B707 side fire), respectively. Temperature predictions are noticeably high, from 80 to 120 seconds in both cases, with a more pronounced difference for test case 3. Modeling is expected to be more challenging for these two test cases because the fire source is placed close to the walls. However, it is important to note that the total number of experiments for these test cases is much lower than that for test case 1; thus, experimental data is also expected to have higher uncertainty. Evidence of this can be found in the contourplots for test case 3 (figure 18); the maximum ceiling temperature is slightly shifted down in the test data, suggesting a possible error in the position of the heat source or a reflection or diversion surface that is not modeled.

The gas temperatures close to the floor were predicted fairly well for test cases 2 and 3 (not shown). Note that the thermocouple tree was kept at the same location for all three test cases conducted in the B707 cargo compartment. In other words, it was located away from the heat source for test cases 2 and 3; thus, possible model errors due to the implementation of radiative source term were expected to be smaller. However, the discrepancy in the gas temperatures close to the ceiling persists for these test cases as well. Similar to the thermocouple tree, wall thermocouples and heat flux sensors were also positioned at the same place for all three test cases. For the corner fire, wall temperatures and heat fluxes were well predicted (not shown). For the side fire, wall temperature and heat flux measured close to the fire source was overpredicted (not shown). Concentrations of CO, CO_2, and smoke agreed reasonably well with the test data for both test cases (see figures 19(a and b) and 20 for the corner test case, and figures 19(c and d) and 21 for the side test case).

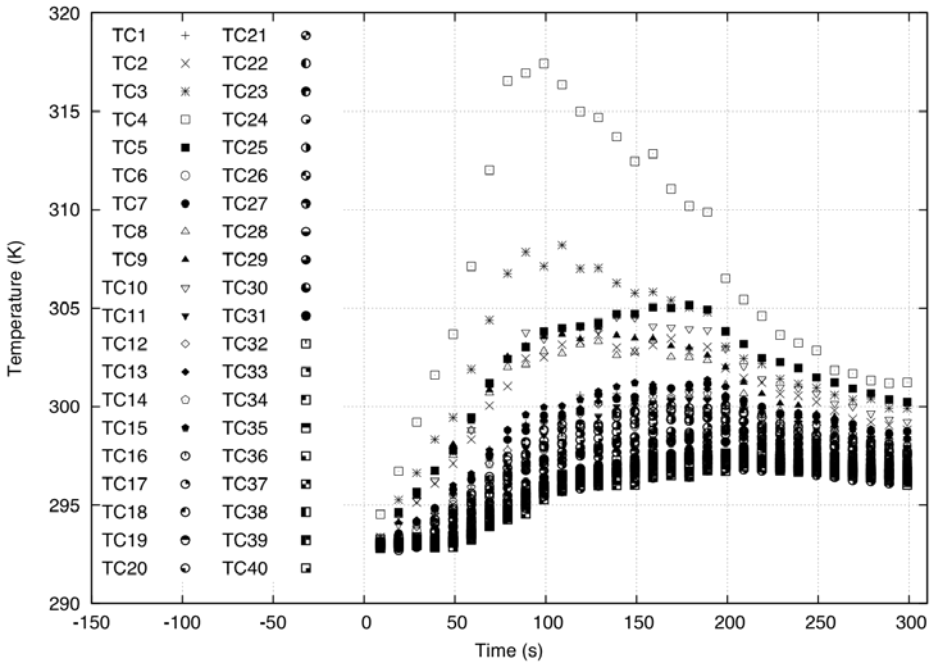

(a) Experimental Data

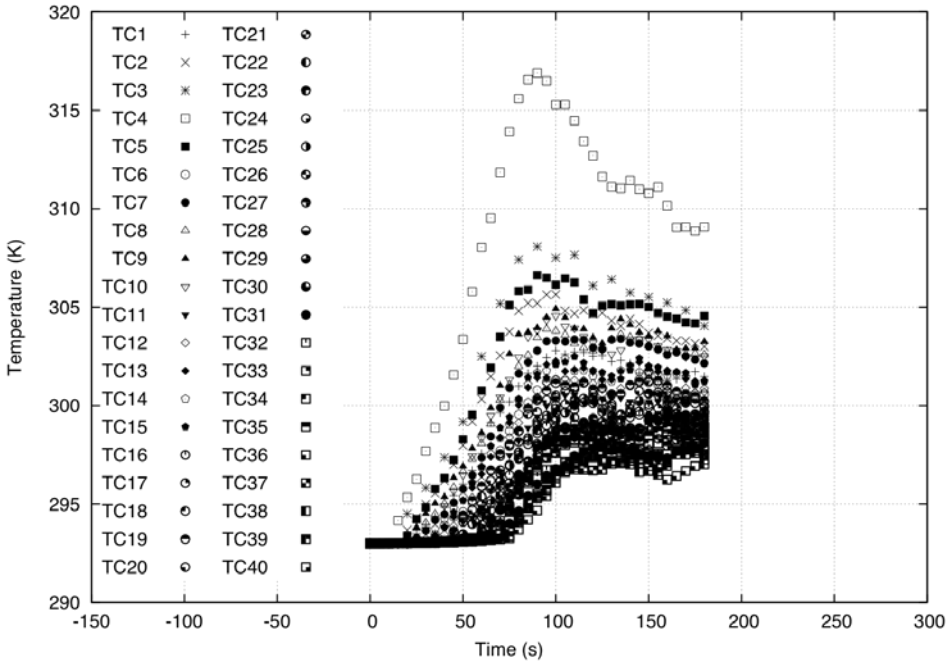

(b) Model (FDS) Predictions

Figure 13. The B707 Corner Fire: Comparisons Between Experimental Data and Model (FDS) Predictions—Time Variation of Time-Averaged Ceiling Gas Temperatures for (a) Experimental Data and (b) Model Predictions

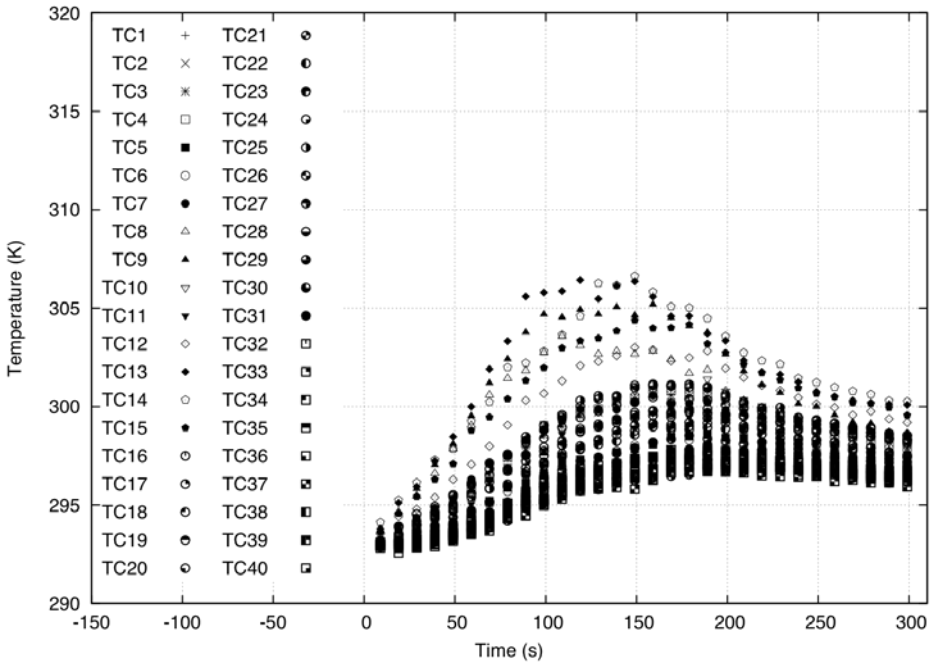

(a) Experimental Data

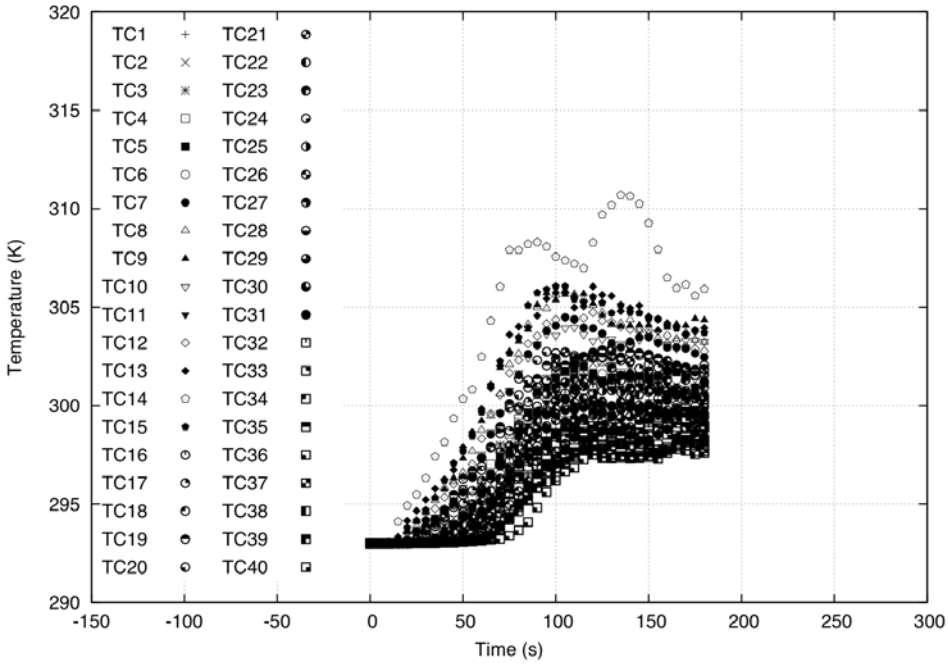

(b) Model (FDS) Predictions

Figure 14. The B707 Side Fire: Comparisons Between Experimental Data and Model (FDS) Predictions—Time Variation of Time-Averaged Ceiling Gas Temperatures for (a) Experimental Data and (b) Model Predictions

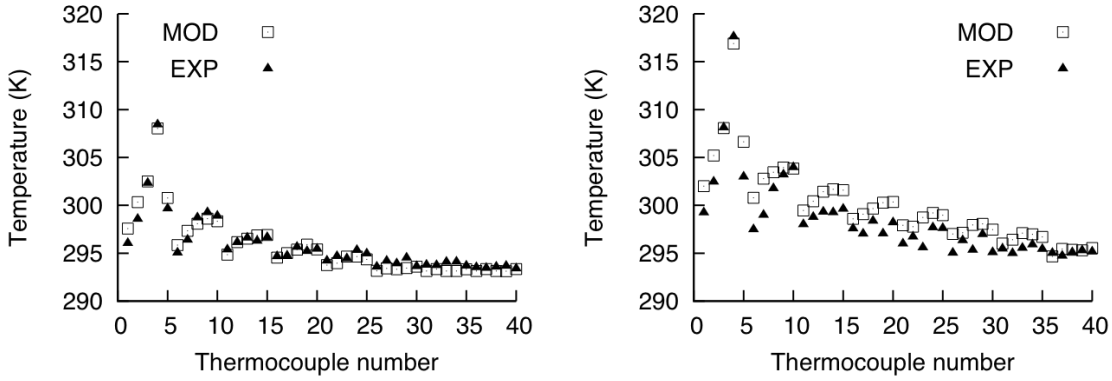

(a) 60 s (b) 90 s

Figure 15. The B707 Corner Fire: Comparisons Between Experimental Data and Model (FDS) Predictions—Spatial Variation of Time-Averaged Ceiling Gas Temperatures at (a) 60 s and (b) 90 s

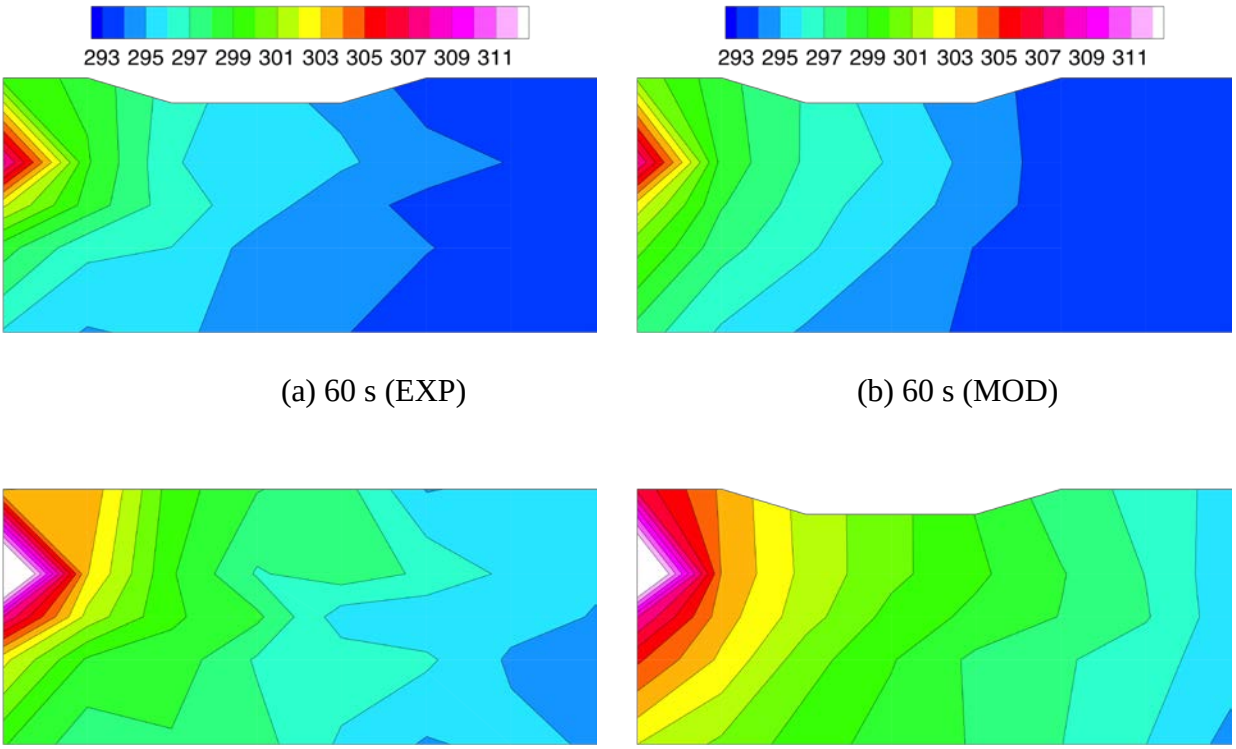

(a) 60 s (EXP) (b) 60 s (MOD)

(c) 90 s (EXP) (d) 90 s (MOD)

Figure 16. The B707 Corner Fire: Comparisons Between Experimental Data and Model (FDS) Predictions—Contourplots of Time-Averaged Ceiling Gas Temperatures at Selected Times for Experimental Data at (a) 60 s and (c) 90 s, and Model Predictions at (b) 60 s and (d) 90 s

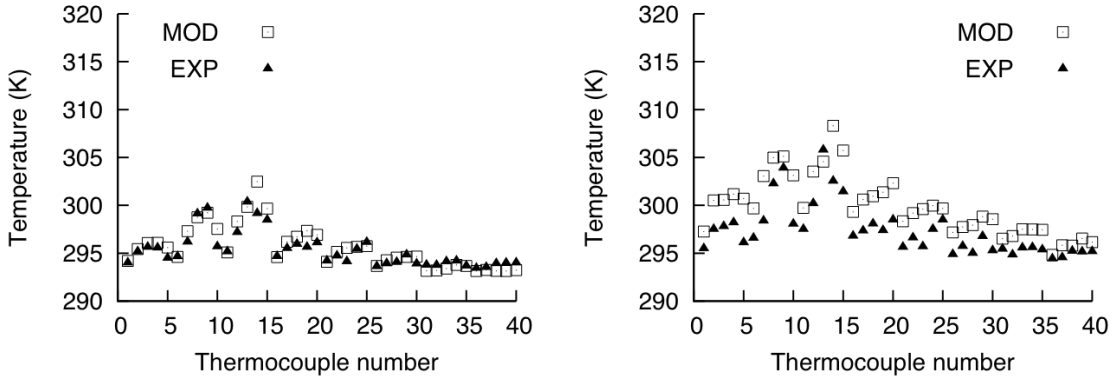

(a) 60 s (b) 90 s

Figure 17. The B707 Side Fire: Comparisons Between Experimental Data and Model (FDS) Predictions—Spatial Variation of Time-Averaged Ceiling Gas Temperatures at (a) 60 s and (b) 90 s

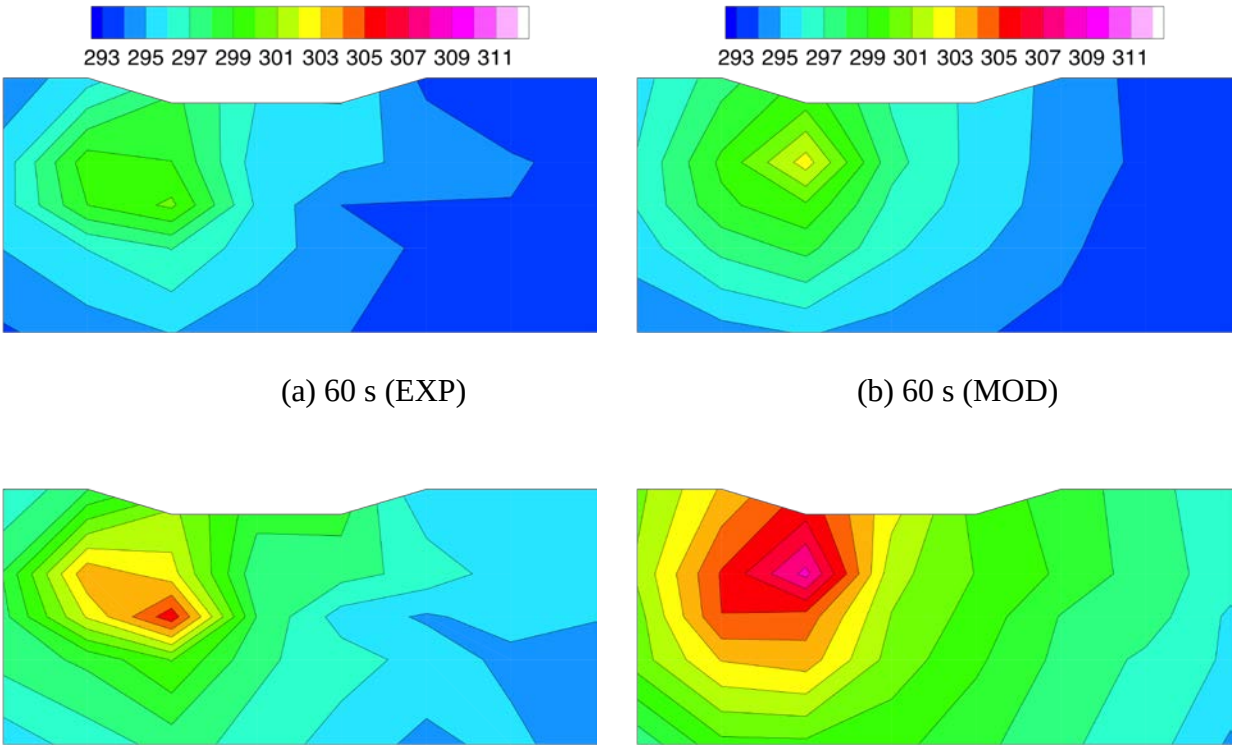

(a) 60 s (EXP) (b) 60 s (MOD)

(c) 90 s (EXP) (d) 90 s (MOD)

Figure 18. The B707 Side Fire: Comparisons Between Experimental Data and Model (FDS) Predictions—Contourplots of Time-Averaged Ceiling Gas Temperatures at Selected Times for Experimental Data at (a) 60 s and (c) 90 s, and Model Predictions at (b) 60 s and (d) 90 s

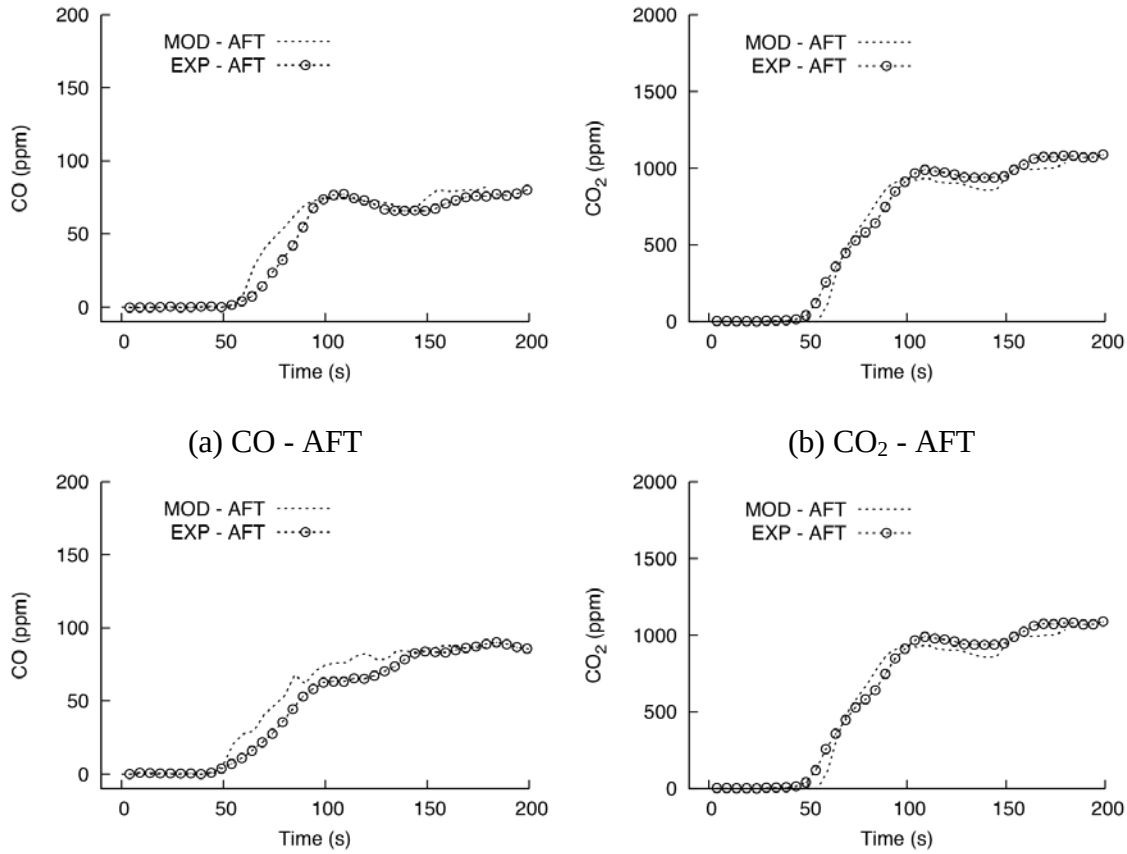

(a) CO - AFT (b) CO_2 - AFT

(c) CO - AFT (d) CO_2 - AFT

Figure 19. The B707 Corner Fire: Comparisons Between Experimental Data and Model (FDS) Predictions—Time Variation of (a) CO and (b) CO_2 Concentrations at AFT Analyzer Location; Side Fire: Comparisons Between Experimental Data and Model (FDS) Predictions—Time Variation of (a) CO and (b) CO_2 Concentrations at AFT Analyzer Location

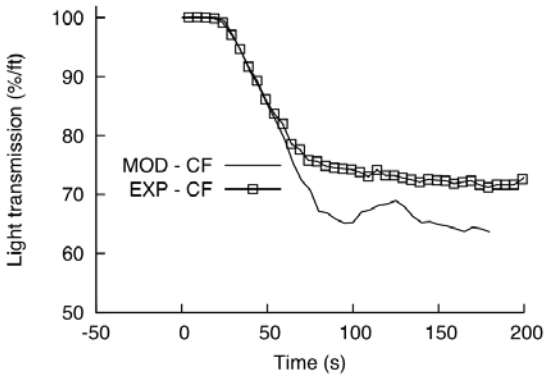

(a) Ceiling - FWD

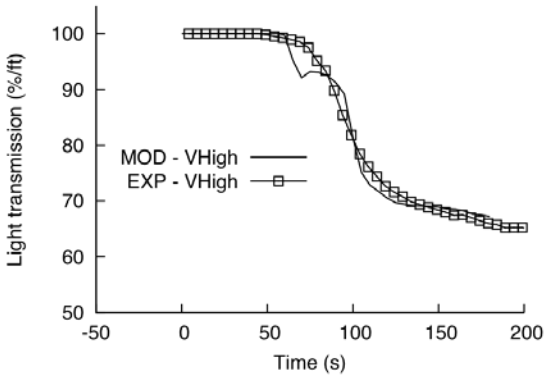

(b) Vertical - HIGH

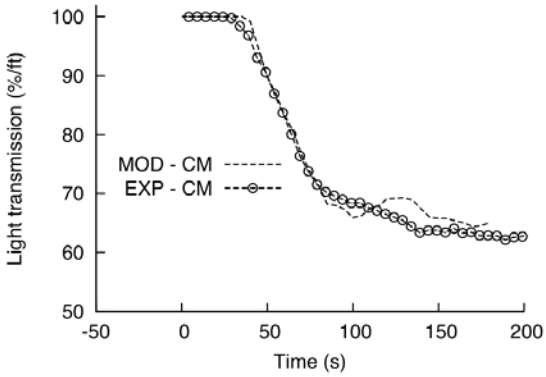

(c) Ceiling - MID

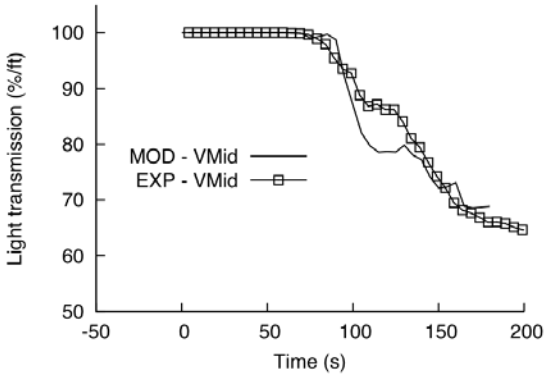

(d) Vertical - MID

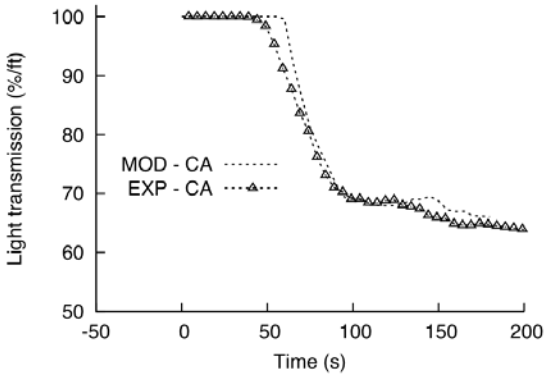

(e) Ceiling - TC36

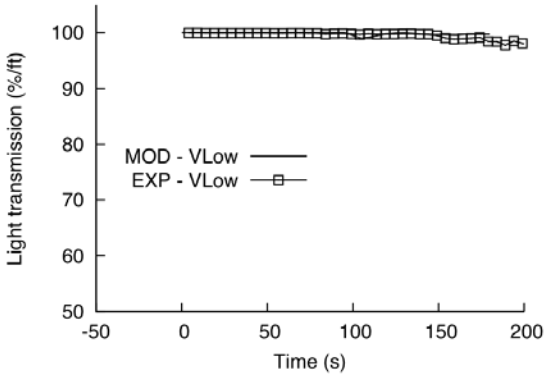

(f) Vertical – LOW

(CF: ceiling forward, CM: ceiling mid, CA: ceiling aft, VHigh: vertical high, VMid: vertical mid, VLow: vertical low)

Figure 20. The B707 Corner Fire: Comparisons Between Experimental Data and Model (FDS) Predictions—Time Variation of Light Transmissions at Ceiling Beam Detectors ((a) Aft, (c) Mid, and (e) TC36) and Vertical Beam Detectors ((b) High, (d) Mid, (f) Low)

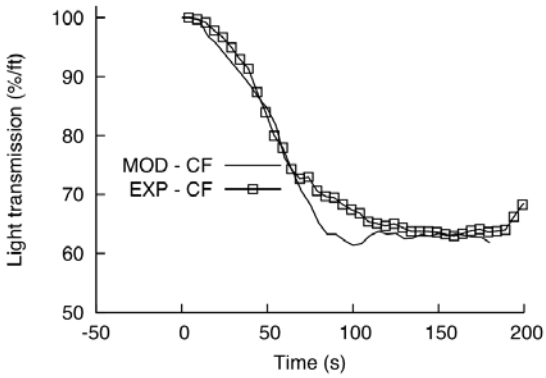

(a) Ceiling - FWD

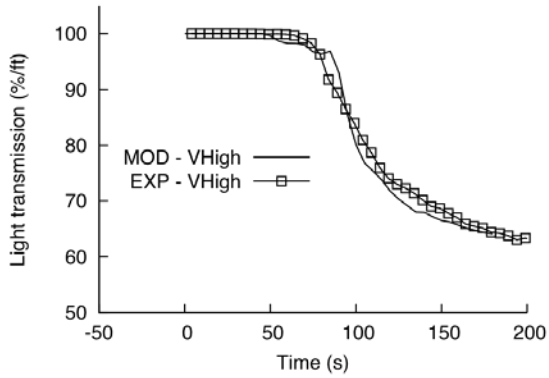

(b) Vertical - HIGH

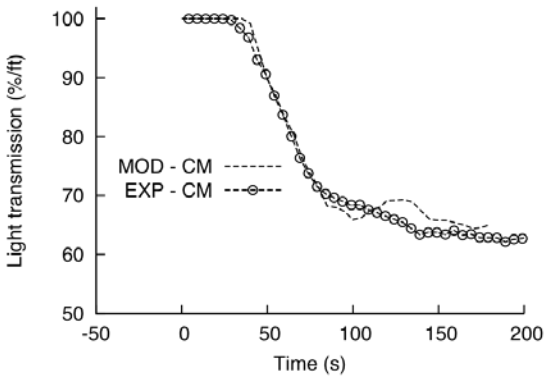

(c) Ceiling - MID

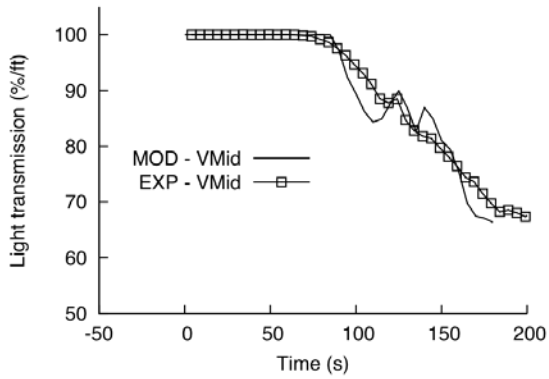

(d) Vertical - MID

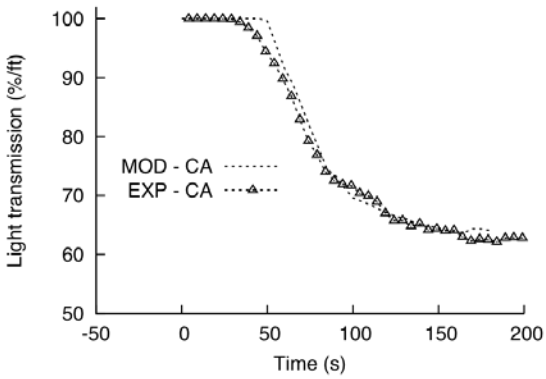

(e) Ceiling - TC36

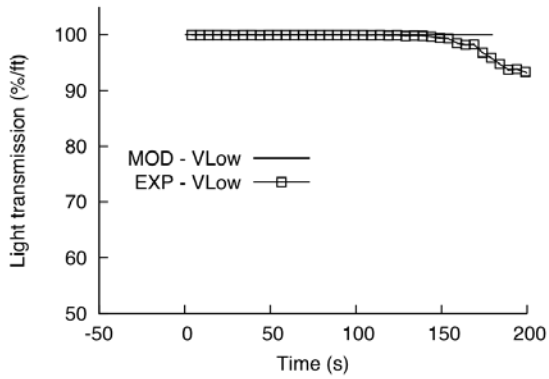

(f) Vertical – LOW

(CF: ceiling forward, CM: ceiling mid, CA: ceiling aft, VHigh: vertical high, VMid: vertical mid, VLow: vertical low)

Figure 21. The B707 Side Fire: Comparisons Between Experimental Data and Model (FDS) Predictions—Time Variation of Light Transmissions at Ceiling Beam Detectors (a) Aft, (c) Mid, and (e) TC36; and Vertical Beam Detectors (b) High, (d) Mid, and (f) Low

Test Case 4—DC10 Base Fire. The spatial variation of ceiling temperatures at arbitrarily selected times are plotted in figures 22 and 23. These figures show that model predictions are 2 to 3K higher for the first 20 thermocouples. Concentrations of CO and CO_2 are reasonably well predicted (figure 24). However, smoke concentrations are not as successful as those obtained previously for the other three test cases (figure 25).

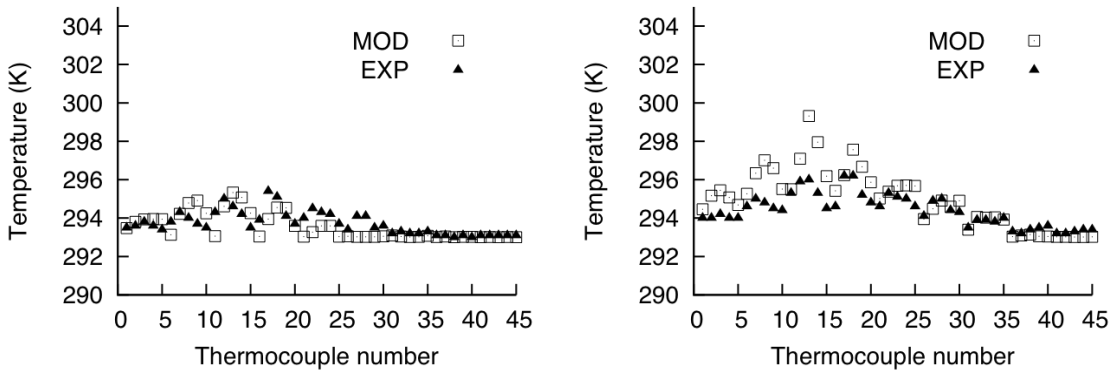

(a) 60 s (b) 90 s

Figure 22. The DC10 Base Fire: Comparisons Between Experimental Data and Model (FDS) Predictions—Spatial Variation of Time-Averaged Ceiling Gas Temperatures at (a) 60 s and (b) 90 s

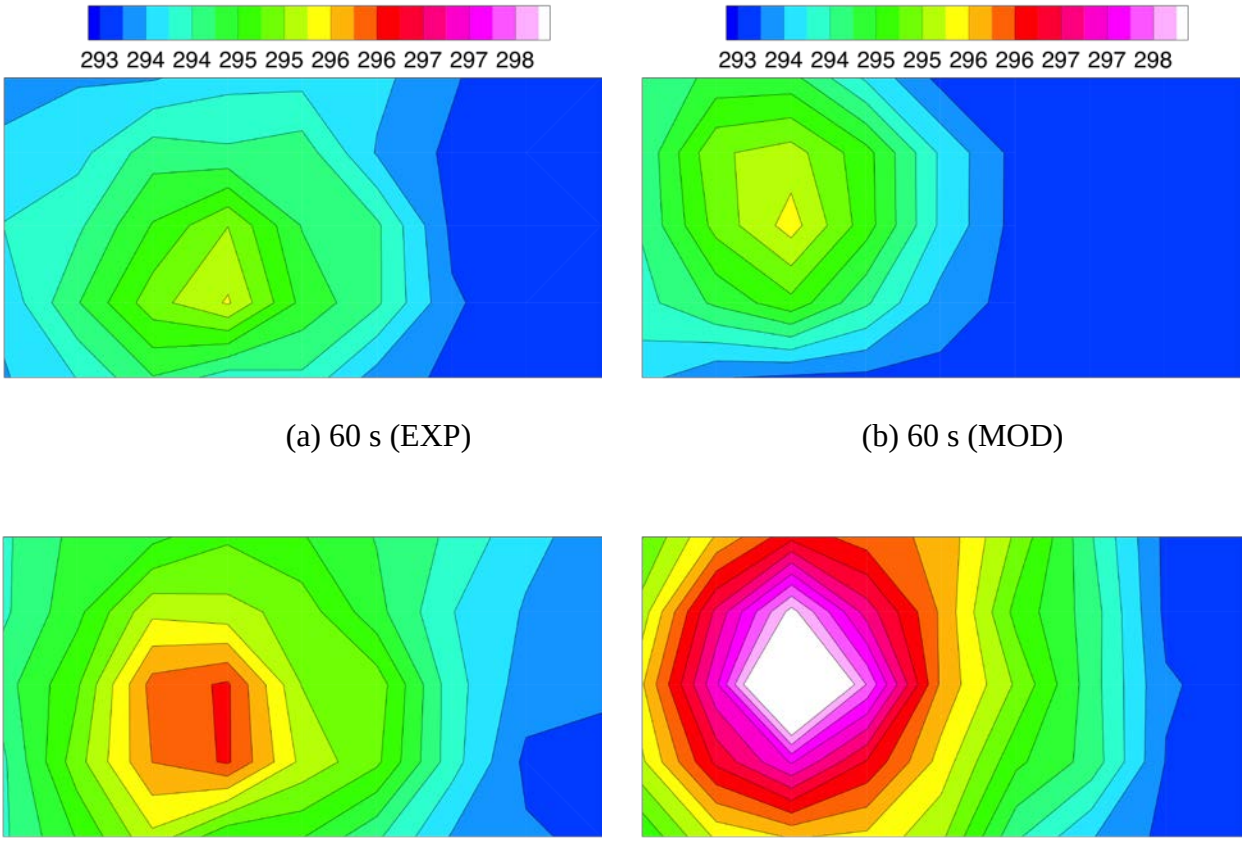

(a) 60 s (EXP) (b) 60 s (MOD)

(c) 90 s (EXP) (d) 90 s (MOD)

Figure 23. The DC10 Base Fire: Comparisons Between Experimental Data and Model (FDS) Predictions—Contourplots of Time-Averaged Ceiling Gas Temperatures at Selected Times for Experimental Data at (a) 60 s and (c) 90 s, and Model Predictions at (b) 60 s and (d) 90 s

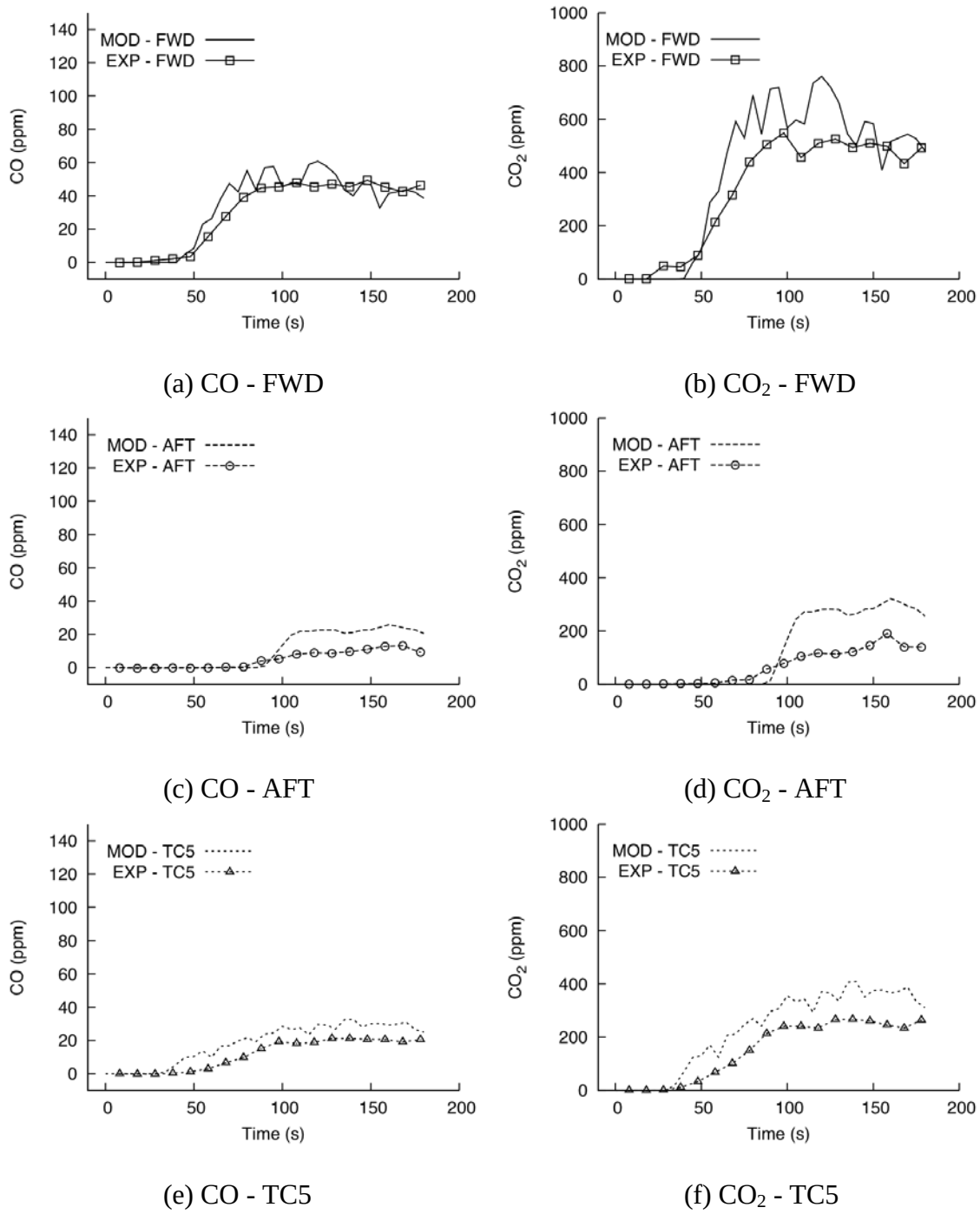

(a) CO - FWD

(b) CO_2 - FWD

(c) CO - AFT

(d) CO_2 - AFT

(e) CO - TC5

(f) CO_2 - TC5

Figure 24. The DC10 Base Fire: Comparisons Between Experimental Data and Model (FDS) Predictions—Time Variation of (a, c, and e) CO and (b, d, and f) CO_2 Concentrations at FWD, AFT, TC5 Analyzer Locations, Respectively

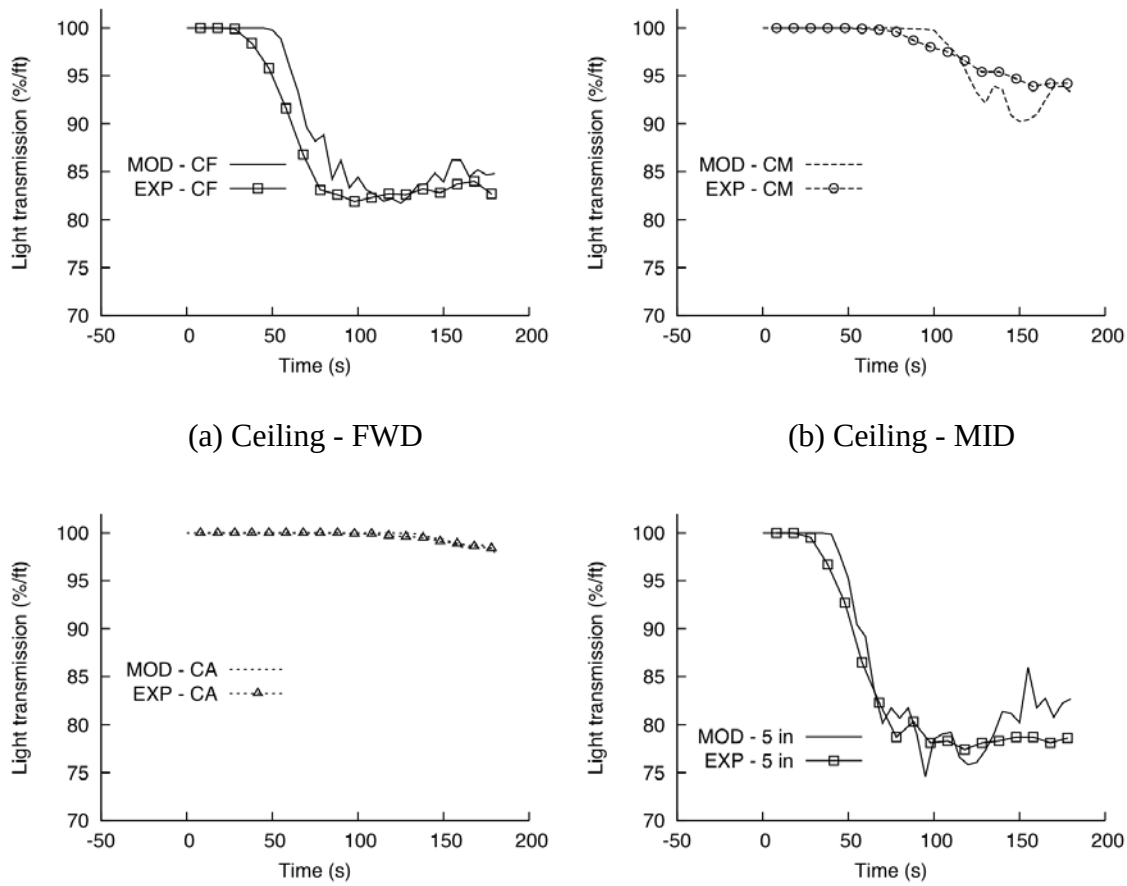

(a) Ceiling - FWD

(b) Ceiling - MID

(c) Ceiling - TC5

(d) Vertical - 5'

(CF: ceiling forward, CM: ceiling mid, CA: ceiling aft, 5' vertical)

Figure 25. DC10 Base Fire: Comparisons Between Experimental Data and Model (FDS) Predictions—Time Variation of Light Transmissions at Ceiling Beam Detectors ((a) Fwd, (b) Mid, (c) TC5) and Vertical Beam Detector (e) 5'

Summary of Model Results. The agreement between model and measurements is summarized in table 3 for all four test cases studied. For the chosen validation metric, its location is also listed in the table—whether the test instrument is located in the ceiling or vertical, and whether it is close to or away from the fire. The qualification of the results were grouped into three categories: good, moderate, and poor (shown with symbols + +, + -, and - -, respectively). For example, model predictions of the ceiling gas temperatures agreed reasonably well with the measurements of test case 1. This is shown in table 3 with the symbols + -, which indicate a moderate agreement between the model and the measurement. On the other hand, the same test case model generated excellent results for CO concentrations; the symbols + + indicate good agreement between the model and the measurement. Finally, the wall temperature close to the fire was overpredicted for test case 1; this is shown in the table with the symbols - - to indicate poor agreement between the model and the measurement. Also, the NA (not applicable) abbreviation is used whenever there is no test data or instrument location is unclear. It is

important to note that the disagreement between the model and the test data is not necessarily an indication of poor model performance; it may also be due to faulty instrumentation or uncertainty in the test data.

Model (FDS) predictions were generally in good agreement with the test data, except for gas temperatures in the vertical and wall temperatures closer to the fire source. Note that it was not possible to eliminate instrumentation errors as the source of any of these discrepancies since the tests were performed almost a decade ago and were not repeated as part of the present study. Furthermore, although radiative fraction was carefully selected by examining fuels with similar soot yields in the literature, it is important to make measurements directly for the FAA fire source used in the full-scale tests. Model results will change drastically if the chosen value for radiative fraction is incorrect.

Table 3. Summary of Agreement Between Model Predictions and Measurements

Metric	Location	Test Case 1 B707 Base	Test Case 2 B707 Corner	Test Case 3 B707 Side	Test Case 4 DC10 Base
Gas temperature	Ceiling Vertical	+ - - -	+ - - -	- - - -	- - N/A
Wall temperature	Close Away	- - + +	+ + + +	- - + +	N/A N/A
Heat flux	Close Away	- - + +	+ + + +	- - + +	N/A N/A
CO concentration CO_2 concentration	Ceiling Ceiling	+ + + -	+ + + +	+ + + +	+ - + -
Smoke concentration	Ceiling Vertical	+ + + -	+ - + -	+ + + -	+ - + -

An alternative method of model evaluation is to construct scatterplots where a linear relationship between the predictions and the experimental data is tested. In scatterplots, one axis is reserved for the predicted value while the other shows the measured one, with the paired data on the equivalency line ($y = x$) indicating the best agreement. For transient problems, it is critical to choose a time instant when the comparisons will be representative of a general trend between the predictions and the measurements. Comparisons of peak (maximum) values are well suited for fire problems as the interest is usually in the amount of increase from a reference value, such as the rise in temperatures/concentrations due to a given fire source. Thus, to attain a general idea of model performance in the current analysis, scatterplots compiled from the peak values for each quantity of interest were examined.

In figure 26, which shows the scatterplots of all variables for all test cases studied, a different color is used for each test case and symbols distinguish the variables (i.e., ceiling temperatures; concentrations of CO, CO_2, and smoke; vertical gas temperatures; and heat fluxes). To enable comparisons in a single plot, dimensionless quantities are needed. Nondimensionalization is done using the maximum value measured in test case 1 for each quantity.

In general, the agreement between the model and the experimental data was within ~20% margin. However, vertical temperatures (shown in filled circles) and heat fluxes (shown in diamonds) were consistently out of this error margin, in addition to the CO and CO_2 concentrations for test case 4.

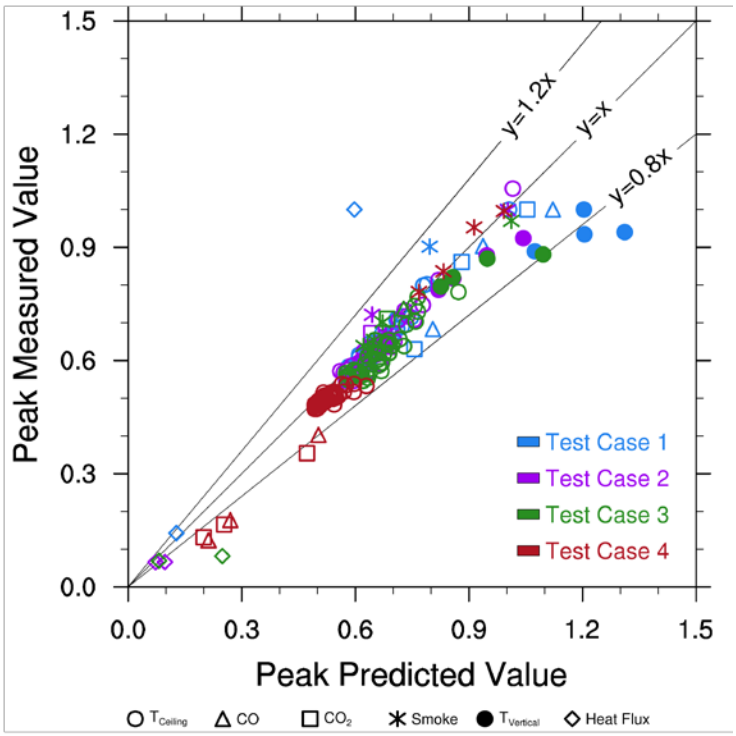

Figure 26. Comparisons Between Experimental Data and Model (FDS) Predictions—Nondimensional Peak Values for Ceiling Gas Temperatures, Smoke and Gas Concentrations, Vertical Gas Temperatures, and Heat Fluxes

For test case 1, the B707 baseline fire scenario, ceiling temperatures (shown as circles) are on the equivalency line, indicating good agreement between the measurements and the predictions. However, all four temperatures measured on the thermocouple tree (shown as filled circles) were overpredicted at close to, or even more than, 20%. In addition, one of the heat fluxes (shown as the diamond) was underpredicted with a large error margin. For test case 2, the B707 corner fire scenario, all variables are estimated within 10% (or even less) of measurements, except for one of the heat fluxes, which was overpredicted. For test case 3, the B707 side fire scenario, a similar behavior was seen with slightly larger error margins. For this test case, the disagreement between the model and the test data for ceiling temperatures increased. Similarly, for test case 4, the DC10 baseline fire scenario, the model overpredicted the ceiling temperatures, and was not as successful at predicting gas concentrations as the other three test cases. Comparisons of vertical temperatures and heat fluxes were not made for test case 4 because the locations of the thermocouple tree and the heat flux sensors are unclear.

CONCLUSIONS

The transport of smoke and hot gases driven by a small fire in an aircraft cargo compartment was modeled using the Fire Dynamics Simulator (FDS) [5] developed by the National Institute of Standards and Technology. Numerical modeling was carried out for two types of compartments: the Boeing 707 (B707) forward cargo compartment that represents a narrow-body compartment with no forced ventilation, and the McDonnell Douglas DC-10 (DC10) below floor cargo compartment that exemplifies a wide-body compartment with a considerable amount of ventilation. Results were compared against the measurements of the full-scale tests conducted at the Federal Aviation Administration (FAA) Technical Center between the years of 2003 and 2004. The experiments consisted of four test cases—three of which were conducted in the B707 compartment and differed only in the location of the fire source, and one conducted in the DC10 compartment. The standardized fire source [6 and 8-10], a compressed resin block containing pellets of various polymers that was developed by the FAA Technical Center, was used in all of the full-scale tests. A separate set of bench-scale tests was also performed for the characterization of the FAA fire source. This cone calorimetry data is used to prescribe the heat release and the production rates of gas species in the model. Solutions are examined for temperatures, gas concentrations, and light transmissions, similar to an earlier study where the uncertainties in the tests were quantified [6].

The grid sensitivity analysis conducted for the B707 test cases showed that convergence was not achieved for resolutions with $D^*/\Delta x_{\min} < 5$, where D^* is the characteristic fire diameter and Δx is the cell size. The B707 simulations presented in this document were conducted with $D^*/\Delta x_{\min} = 10$. For the DC10, a complete grid sensitivity analysis was not possible because of limited computational resources. The presented results for DC10 simulations were achieved with $D^*/\Delta x_{\min} = 5$.

The initial simulation results showed an increase in the ceiling gas temperatures with time [17] and low heat fluxes in comparison to the measured values. Two modifications to the flow solver were made; one drastically changed the convective heat fluxes near the ceiling and considerably improved the model predictions.

For all three fire scenarios of the B707 cargo compartment, concentrations of smoke, CO, and CO_2 were predicted within or close to the experimental uncertainty. The ceiling temperatures, except for that of the side fire scenario, were estimated within 1 to 2K of the experimental mean. However, predictions at the tree thermocouples, particularly those close to the ceiling, were high in comparison to the measurements. Wall temperatures close to the fire were predicted lower in the base fire scenario and higher in the side fire scenario. Overall, B707 model predictions were in good agreement with the test data. The maximum deviation between model and the test data was observed for the side fire scenario, for which the heat source was moved close to the side wall. The source of the disagreement with the model predictions for this test case may be due to possible wrong placement of the fire source. It is suspected that the resin block in the side fire scenario was located closer to the center of the compartment, rather than the recorded location. Furthermore, the top thermocouple on the thermocouple tree consistently started with high temperature readings, unlike all other thermocouple measurements, and was likely to be faulty.

This may explain the difference between model and the test data for the upper two thermocouples on the tree. However, the disagreement for the other two thermocouples close to the floor was likely due to the implementation of radiation source term in the model. For the fire scenario of the DC10 cargo compartment, the ceiling gas temperatures were estimated higher than that of the measurements, while the light transmissions and gas concentrations agreed reasonably well.

In summary, there was reasonably good agreement between FDS predictions and the test data. For the cases where the model failed to predict the test data well, it is important to revisit not only the model, but also the measurements. Thus, it is strongly recommended that the experiments and the modeling be done in tandem so that possible errors associated with both can be scrutinized and eliminated. It is also important to support model input with direct measurements. For example, radiative fraction of the fuel source is not known, but is estimated based on that of similar fuels found in the literature. This is a critical model input that may change the model solutions drastically.

REFERENCES

1. "Federal Aviation Regulation (FAR), Part 25, Section 858—Cargo or Baggage Compartment Smoke or Fire Detection," FAR 25, Federal Aviation Administration, September 1980.

2. Cleary, T. and Donnelly, M., "Aircraft Cargo Compartment Fire and Nuisance Source Tests in the FE/DE," *Proceedings of the 12th International Conference on Automatic Fire Detection*, National Institute of Standards and Technology, Gaithersburg, Maryland, 2001.

3. Blake, D., "Aircraft Cargo Compartment Smoke Detector Alarm Incident on US-Registered Aircraft, 1974-1999," FAA Report DOT/FAA/AR-TN00/29, June 2000.

4. Cleary, T. and Grosshandler, W., "Survey of Fire Detection Technologies and System Evaluation/Certification Methodologies and Their Suitability for Aircraft Cargo Compartments," NIS-TIR 6356, National Institute of Standards and Technology, July 1999.

5. McGrattan, K.B., Hostikka, S., Floyd, J., Baum, H.R., Rehm, R.G., Mell, W., and McDermott, R., "Fire Dynamics Simulator - Technical Reference Guide," NIST Special Publication 1018-5, National Institute of Standards and Technology, October 2010, http://www.fire.nist.gov/fds/

6. Suo-Anttila, J., Gill, W., Luketa-Hanlin, A., and Gallegos, C., "Cargo Compartment Smoke Transport Computational Fluid Dynamics Code Validation," FAA Report DOT/FAA/AR-07/27, July 2007.

7. Suo-Anttila, J., Gill, W., Luketa-Hanlin, A., and Gallegos, C., "Computational Fluid Dynamics Code for Smoke Transport During an Aircraft Cargo Compartment Fire: Transport Solver, Graphical User Interface, and Preliminary Baseline Validation," FAA Report DOT/FAA/AR-03/49, October 2003.

8. Blake, D. and Suo-Anttila, J., "Aircraft Cargo Compartment Fire Detection and Smoke Transport Modeling," *Fire Safety Journal*, Vol. 43, No. 8, 2008, pp. 576–582.

9. Filipczak, R., Blake, D., Speitel, L., Lyon, R., and Suo-Anttila, J., "Development and Testing of a Smoke Generation Source," *Proceedings of the Fire and Materials Conference*, San Francisco, California, 2001.

10. Speitel, L.C., "Fourier Transform Infrared Analysis of Combustion Gases," *Journal of Fire Sciences*, Vol. 20, No. 5, September 2002, pp. 347–433.

11. Baum, H., Ezekoye, O., McGrattan, K., and Rehm, R., "Mathematical Modeling and Computer Simulation of Fire Phenomenon," *Theoretical and Computational Fluid Dynamics*, Vol. 125, No. 6, 1994.

12. Smagorinsky, J., "General Circulation Experiments With the Primitive Equations. I. The Basic Experiment," *Monthly Weather Review*, Vol. 91, No. 3, March 1963, pp. 99–164.

13. Sweet, R., "Direct Methods for the Solution of Poisson's Equation on a Staggered Grid," *Journal of Computational Physics*, Vol. 12, 1973, pp. 422–428.

14. Tewarson, A., "Smoke Point Height and Fire Properties of Materials," NIST-GCR-88-555, National Institute of Standards and Technology, December 1988.

15. McGrattan, K.B., McDermott, R., Hostikka, S., and Floyd, J., "Fire Dynamics Simulator—User's Guide," NIST Special Publication 1019-5, National Institute of Standards and Technology, September 2010, http://www.fire.nist.gov/fds/

16. Mulholland, G.W., *SFPE Handbook of Fire Protection Engineering*, "Smoke Production and Properties," National Fire Protection Association, Quincy, Massachusetts, 2002, pp. 258–268.

17. Oztekin, E.S., Blake, D., and Lyon, R.E., "Flow Induced by a Small Fire in an Aircraft Cargo Compartment," 50th AIAA Applied Aerospace Sciences Meeting and Exhibit, AIAA, Nashville, Tennessee, 2012.